Petrographic and geochemical features of sinkhole-filling deposits associated with an erosional unconformity on Grand Cayman

Ting Liang*, Brian Jones

Department of Earth and Atmospheric Sciences, University of Alberta, Edmonton, Alberta, T6G 2E3, Canada

Corresponding author: E-mail address: tliang1@ualberta.ca *(T. Liang)*

ABSTRACT

On Grand Cayman, exposures of dolostones belonging to the Cayman Formation (Miocene) represent an erosional unconformity that has been developing since the late Pliocene (~3.6 Ma). Sinkholes that developed during this time have remained open or become partly to fully filled with various combinations of rootcrete, breccias, loose limestone and dolostone lithoclasts, and white, red and orange limestones. These sinkhole-filling deposits have different geochemical attributes to the Neogene and Pleistocene marine carbonates that form the bedrock of the island. The deposits in the sinkholes formed in response to the variations of sea level, climate, exposure, and vegetation that developed during the period when the erosional unconformity was developing.

The rootcrete, oncoids, red and orange limestones are terrestrial in origin, whereas the limestone and dolostone lithoclasts and white limestones are derived from marine deposits. On the erosional unconformity, intense root activity led to the formation of rootcrete and terrestrial oncoids but also selectively blackening reworked marine carbonates. The red and orange limestone matrices, which formed under more arid conditions, contrast with the other sinkhole-filling deposits that formed during periods when the climate was semi-arid to humid. The distinctive REE signatures of the sinkhole-filling deposits, which are different from those of the bedrock limestones and dolostones, can probably be attributed to trace amount of terra rossa and/or airborne Saharan-derived dust that are present in those deposits. .

Keywords: Rootcrete; Black limestone lithoclasts; Terra rossa; Sinkhole; Unconformity; Cayman Islands

1. Introduction

Erosional unconformities in carbonate successions typically represent long periods of subaerial erosion that are accompanied by loss of the rock record, vadose diagenetic and/or pedogenetic alteration, and the formation of surface and subsurface karst (Esteban and Klappa, 1983; James and Choquette, 1990; Tucker, 1990; Clari et al., 1995; Hillgärtner, 1998; Sattler et al., 2005; Alonso-Zarza and Wright, 2010). Assessing the loss of strata is difficult because there is generally no physical record left. In some cases, however, this problem can be partly addressed by examining the lithoclasts and associated sediments that are found in sinkholes and caves that formed during the period of exposure. Studies like those by Daugherty et al. (1987), Smart et al. (1988), Jones (1992b), and Miller et al. (2012), however, are scarce because there are few examples where sinkholes have been filled by carbonate rather than fluvial siliciclastic sediments (Ford, 1988).

Grand Cayman is a carbonate island that is devoid of surface fluvial systems and lack siliciclastic sediments. On the eastern half of Grand Cayman, dolostones of the Cayman Formation (Miocene) have been exposed since the late Pliocene (~3.6 Ma), when the overlying Pedro Castle Formation was lost to subaerial erosion (Wignall, 1995; Zhao and Jones, 2013; Liang and Jones, 2014). The exposed upper surface of the Cayman Formation, which is an unconformity surface that is still developing, is characterized by numerous sinkholes. Some of these sinkholes, which are up to 30 m in diameter and 10 m deep, remain open whereas others are filled with a variety of deposits that include laminar rootcrete, breccias, loose limestone and dolostone lithoclasts, and white, red and orange limestones. Information derived from these deposits provide some insights into the processes that have been operative over the last 3.6 ma. while this unconformity has developed. Some of these sinkhole-filling deposits have been described in terms of their spatial development and petrography (Jones and Smith, 1988; Jones, 1991, 1992a, 1992b; Alonso-Zarza and Jones, 2007). This study builds on that work by assessing the deposits through the integration of stable isotope analyses, trace element analyses, and examining the distribution of the Rare Earth Elements (REE). Using all of this information, this paper (1) compares the petrographic and geochemical features of the different types of sinkhole-filling deposits, (2) compares the geochemical signatures of the sinkhole-filling deposits with the limestones and dolostones of the bedrock found on the island, and (3) determines the provenance and sequential development of the sinkhole-filling deposits. In particular, it examines the possibility that carbonates that formed in marine or non-marine environments may be characterized by different REE signatures.

2. Terminology

Calcrete that is associated with roots has been referred as laminar calcrete (Wright et al., 1988; Alonso-Zarza, 1999), rhizogenic calcrete (Wright et al., 1995), calcified root mat (Wright et al., 1988), and rootcrete (Jones, 1992a, 1992c). Wright et al. (1995, p. 144) originally defined rhizogenic calcrete as "… calcretes which are composed largely or wholly of textures which are interpretable as due to the calcification on, in or around roots". In their definition, rhizogenic calcrete includes vertical and horizontal root mats (Wright et al., 1995, 1997). The term rootcrete was used to describe calcrete crusts that covered the surfaces of cavities that had been created by the activities associated with plant roots (Jones, 1992a).

The term "terra rossa", first used in soil science by Kubiëna (1953), has been applied to (1) red, shallow, undifferentiated soils that are associated with carbonate or calcareous material, (2) red material which is transitional between weathered carbonate and new soils, and (3) any red soil in the Mediterranean region (Stephens, 1953; Stace, 1956). In geological situations, "terra rossa" has generally been applied to any reddish, clay-rich soils that lie on limestones or dolostones (e.g., Torrent, 1995; Durn et al., 1999, 2001, 2013; Durn, 2003; Muhs and Budahn, 2009; Muhs et al., 2010), whereas reddish, Al-rich soils are generally referred to as bauxite (e.g., Ahmad and Jones, 1969; Muhs and Budahn, 2009). The chief minerals found in terra rossa are variable, but commonly include clay minerals, such as illite, kaolinites, chlorite, and various combinations of quartz, feldspar, and mica (e.g., Macleod, 1980; Garcia-Gonzalez and Recio, 1988; Moresi and Mongelli, 1988; Boero et al., 1992; Bronger and Bruhn-Lobin, 1997; Durn et al., 1999; Muhs and Budahn, 2009). Calcite and dolomite are present in some of these deposits.

Terrestrial oncoids are laminated coated grains, up to 85 mm in diameter, that develop through microbially-mediated processes in a vadose setting (Wright, 1989; Jones, 1991, 2011). The term "micrite", in this study, is applied to carbonate crystals that are less than 4 μm long (Folk, 1974; Reid and MacIntyre, 1998).

3. Geological setting

The Cayman Islands, comprising Grand Cayman, Cayman Brac and Little Cayman, are isolated oceanic islands located on the Cayman Ridge in the Caribbean Sea (Fig. 1). To the south of these islands lies the Oriente Transform Fault that defines the boundary between the North American Plate and the Carribbean Plate. Grand Cayman is located to the northeast of the Mid-Cayman rise, which is an active spreading centre (DeMets and Wiggins-Grandison, 2007). Although located in a tectonically active area, Grand Cayman seems to have remained tectonically stable since the Miocene (Zhao and Jones, 2012, 2013; Liang and Jones, 2014).

The Tertiary carbonate succession on the Cayman Islands was originally assigned to the Bluff Limestone (Matley, 1926), which was subsequently renamed as the Bluff Group by Jones et al. (1994a, 1994b). The Bluff Group is composed of the unconformity-bounded Brac

Formation (Lower Oligocene), Cayman Formation (Middle Miocene), and Pedro Castle Formation (Pliocene) (Fig. 2). The Ironshore Formation (Pleistocene) unconformable overlies the Bluff Group (Fig. 2). The Pedro Castle Formation, which used to cover all of Grand Cayman, has been largely removed from the eastern part of Grand Cayman by subaerial erosion over the last 3-4 million years. As a result, the Cayman Formation is widely exposed over much of the eastern half of Grand Cayman (Fig. 1). Dolomitization of the Bluff Group took place during the late Miocene and early Pliocene (Jones and Luth, 2003; MacNeil and Jones, 2003; Zhao and Jones, 2012, 2013).

The Cayman Formation is formed largely of finely crystalline, fabric retentive dolostones that contain numerous fossils, including corals, bivalves, gastropods, red algae, foraminifera, *Halimeda*, and rhodoliths (Jones, 1994; Jones and Hunter, 1994; Wignall, 1995; Der, 2012). The overlying Pedro Castle Formation is formed of limestones and finely crystalline, fabric-retentive dolostones with free-living corals, foraminifera, red algae, and rhodoliths, along with rare colonial corals, echinoids, and bivalves (Jones, 1994; Jones and Hunter, 1994; Wignall, 1995; Arts, 2000; MacNeil, 2001). The Ironshore Formation is formed of friable limestones that contain numerous, well-preserved corals, bivalves, and gastropods (Jones, 1994; Coyne, 2003; Vézina, 1997; Vézina et al., 1999; Li and Jones, 2013).

4. Methodology

Sinkholes are common features of the phytokarst that characterizes much of the eastern part of Grand Cayman and the uplifted core of Cayman Brac (Fig. 3A, B). For this study, attention was focused largely on the southeast corner of Grand Cayman, because that area (1) has numerous open and filled sinkholes (Fig. 3C), (2) has been largely cleared of vegetation, (3) includes a small quarry that provides some vertical sections through the sinkholes (Fig. 3D), and

(4) is easily accessible. Similar outcrops at other localities yielded a wide variety of different sinkhole- filling sediments (Fig. 3E-H). During study of the sinkholes and sinkhole-filling deposits in the field, 59 hand samples were collected for detailed study. This included five rootcrete samples that were collected from SQW on Cayman Brac (Fig. 1C). Thirty-three large (7.5×5 cm) thin sections were made from samples that were first impregnated with blue epoxy.

Small fracture samples (13 samples) for scanning electron microscope (SEM) analysis were carefully extracted from various samples and mounted on SEM stubs using double-sided tape and/or silver conductive glue and sputter coated with a very thin layer of gold or chrome. SEM analyses were done on a JOEL Field Emission SEM (JOEL 6301F) with an accelerating voltage of 5kV being used for imaging. The elemental composition of selected spots was determined by Energy-dispersive X-ray (EDX) analysis (Priceton Gamma-Tech X-RAY) with an accelerating voltage of 20 kV.

Powdered samples (75-150 μm) of the different components in the samples, obtained by drilling with a 2 mm diameter drill tip, were used for X-ray diffraction (XRD) analysis and geochemical analyses. Eighty-five samples were analyzed on a Rigaku Ultima IV Powder XRD system that was run at 38 kV and 38 mA using an Ultima IV X-ray generator with a Co tube. All scans were run from 5° to 90° 2θ at a speed of 2° θ/min. Using the same samples, oxygen and carbon stable isotopes were determined for 80 calcite and 21 dolomite samples. Following the method of McCrea (1950), the calcite samples were reacted with 100% phosphoric acid at 25 ºC for 1-2 hours, whereas the dolomite samples were reacted with 100% phosphoric acid for 2-3 days at 25 ºC at the University of Alberta's Stable Isotope Laboratory. The extracted CO_2 gas was introduced into a Finnigan-MAT 252 isotope mass spectrometer for analysis of the $\delta^{13}C$ and $\delta^{18}O$, which are reported relative to the Pee Dee Belemnite (PDB) standard normalized to NBS-

18 in the per mil (‰). Analytical reproducibility was 0.05 ‰ for $\delta^{13}C$ and $\delta^{18}O$. The oxygen isotope values of the dolostones were corrected for the phosphoric acid fractionation.

Powdered samples weighing more than 0.2 g (81 samples) were analyzed for their trace elements contents (such as Mn, Fe, Al and REE) in the Radiogenic Isotope Laboratory at the University of Alberta. Those samples were first digested in 10 ml 8N HNO_3. Then, 1 ml of the solution was diluted with 8.8 ml deionized water and 0.1 ml HNO_3 and 0.1 ml of an internal standard (Bi, Sc, and In). A Perkin Elmer Elan 6000 quadrupole inductively coupled plasma mass spectrometer (ICP-MS) was used to analyze the trace elements and REE in the diluted solution. The detection limits for the trace elements are from 0.01 ppm for Th to 5 ppm for P. The REE+Y distribution patterns and La/Yb-Sm/Yb parameters in these samples are illustrated by normalizing each REE+Y concentration against Post-Archean Average Shale (PAAS) (McLennan, 1989).

5. Results

5.1. Sinkholes

Numerous sinkholes are found in the Cayman Formation that is exposed on the eastern half of Grand Cayman (Matley, 1926; Doran, 1954; Stoddart, 1980; Jones et al., 1984; Jones and Smith, 1988) and the central core of Cayman Brac (Fig. 3A, B). On Grand Cayman, the circular to subcircular sinkholes are 1–30 m in diameter and 1–10 m deep (Doran, 1954; Jones and Smith, 1988; Jones, 1989, 1992b) with many being water-filled. On Cayman Brac some of the open sinkholes are at least 18 m deep (Fig. 3B). Based on criteria developed by Cramer (1941) and Ford and Williams (2007), these sinkholes probably originated through dissolution because (1) there are no caves connecting to the bottoms of sinkholes, and (2) fracturing and rupture of the surrounding bedrock are rare.

Numerous sinkholes on Grand Cayman and Cayman Brac were subsequently filled with terra rossa and colonized by various plants, including many of the native trees. Processes association with the plant roots have modified the many of the sinkholes and mediated the formation of a wide variety of deposits. Thus, many sinkholes, like those found on the southeast corner of Grand Cayman are now partly or totally filled with rootcrete, breccia, red and orange limestones, speleothemic calcite, and modern corals and shells (Fig. 3). In this area, many generations of sinkholes are evident with younger ones commonly cross-cutting the older ones.

5.2. Sinkhole-filling deposits

Sinkholes developed in the white dolostones of the Cayman Formation are open (Fig. 3B, C) or filled with a diverse array of rootcrete, breccia, speleothem calcite, and modern corals and shells (Figs. 3, 4). There is no recognizable pattern to the distribution of the different types of sediments (Fig. 5).

5.2.1. Rootcrete

Rootcrete is a laminated calcareous crust, up to 8 cm thick, that follows the contour of the cavity created by roots and/or root hair (Fig. 4, 6, 7). XRD analysis showed that all laminae in the rootcrete, which are up to 2 mm thick, are composed largely of low-Mg calcite. These laminae are highlighted by their black and red colours, which reflect variations in trace element concentrations (Figs. 4, 6). EDX analyses on the SEM show that the black laminae typically contain Mn and Fe (Figs. 7A, 7B, 8A), whereas the red laminae contain Al, K, Fe, and Si (Figs. 7D-H, 8B-E). SEM analyses show that the rootcrete is formed mainly of anhedral to subhedral micrite (< 4 μm long) and euhedral microspar (5-15 μm long), along with minor amounts of Mn precipitates, Fe precipitates, chlorite, feldspar, quartz, and zeolites(?) (Fig. 7A-H). The micrite appears to have formed as the original groundmass, whereas the microspar formed as a cement in the small pores that once existed in the micrite. Fossils in the rootcrete include modern aragonitic gastropod and bivalve shells, which show no evidence of alteration. Borings are evident in some of the biofragments (Fig. 7C). Voids in the rootcrete, up to 0.2 mm long, are commonly lined with fiber calcite crystals that are up to 0.4 μm diameter and 15 μm long (Fig. 7M, 7N).

Alveolar-septal structures are common features of the black and red rootcrete lamina (Fig. 6). The arcuate micritic septa (up to 0.1 mm thick) define irregular-shaped voids that are generally < 1 mm in diameter. Beside spar calcite cement, fillings in those voids vary between different laminae. In the black laminae, for example, Mn-rich reticulate coatings, bladed crystals, or fuzzy coatings are common (Fig. 7A, 7B). The morphology of the very small Fe precipitates, which are present in some of these deposits, cannot be resolved.

In the red laminae, the voids are partly filled by spherical to vaguely laminated elliptical peloids (up to 0.4 mm in diameter) and, in some cases, feldspar, quartz, rare zeolites (?), and dolomite (Figs. 6B, 6F, 7D-G). Some of the vaguely laminated peloids contain spar calcite cement inside them (Fig. 6F). SEM and EDX analyses show that the peloids are formed of micrite and minor amounts of chlorite (Figs. 7H, 8E). Compared to the micrite that forms the alveolar septa, the peloids appear to contain more chlorite. In some samples, the chlorite forms rims composed of platelets that are arranged perpendicular to the peloid surface (Fig. 7H). In other samples, the chlorite is found as individual plates or fibers that are < 2 μm long (Fig. 7A). Euheral feldspar crystals, up to 5 μm long, subhedral quartz crystals (up to 9 μm long), and zeolites (up to 25 μm long) are present in some of the red laminae (Fig. 7D-G). Euhedral to subhedral dolomite crystals, up to 15 μm long, are randomly distributed in some of the rootcrete from localities HRQ and SQW (Fig. 7E).

All laminae in the rootcretes, irrespective of colour, contain numerous calcified spores and filaments. Spherical spores, 0.9-1.3 μm in diameter, are commonly embedded in the calcite cement and/or associated with the fiber calcite. Based on their surface morphology, three types of spores, which are similar in size, are evident. Type I (Fig. 7J) is morphologically akin to the "ovate to spherical cocci having smooth surfaces" described by Jones (2011, his Fig. 9F). Type II (Fig. 7K) is similar to the "smooth spore with radiating spines" described by Jones (1991, his Fig. 9E, 2011, his Fig. 9B). Type III (Fig. 7L) is comparable to the "smooth spores with pores" described by Jones (1991, 2011, his Fig. 9M). Many of these spores have one main opening (< 100 nm) that may be an attachment collar.

The calcified filaments, commonly found in the voids or among fiber calcite crystals, include three morphological types. Type I and Type II are non-branching filaments that are at least 15 μm long and up to 1 μm in diameter (Fig. 7M, 7N). Following the descriptions of the reticulate filaments found on the Cayman Islands (Jones, 1991, 2009, 2010b, 2011), Type I is characterized by diamond and spiral chambers (Fig. 7M), whereas Type II is characterized by isolated surface spines (Fig. 7N). Type III, up to 1 mm long and 1~2 μm in diameter, is a branching filament that has been completely replaced by euhedral calcite crystals (Fig. 7O).

The morphological attributes of those spores and filaments are considered to be taxa-specific because the different types are commonly intertwined with each other. Based on morphological features, the spores and filaments found in sinkholes are similar to those found in cave pearls (Jones, 2009), in notch speleothems (Jones, 2010a), cave speleothems (Jones, 2010b) and terrestrial oncoids (Jones, 2011). Those spores have been allied with actinomycetid spores (e.g., Tresner et al., 1961; Dietz and Mathew, 1969, 1971; Miyadoh et al., 1997), whereas the taxonomic affinity of filamentous microbes remains open to debate.

5.2.2. Breccia

Many of the sinkholes are filled with various types of breccia (Fig. 3D, F, G, 5). The lithoclasts are formed of dolostone or limestone. The limestone lithoclasts are further divided, based on color, into white and black/grey types. The limestone matrices are divided on the basis of color into white, red, and orange. The white limestone matrices are further divided into the skeletal and oncoid types. Different combinations of lithoclasts and matrices give rise to a diverse array of breccias.

The sub-angular to sub-rounded white dolostone lithoclasts, up to 6 cm long and 4 cm wide, (Fig. 3G) are formed of very finely crystalline dolomite and commonly characterized by numerous fossil mouldic cavities after corals, bivalves, foraminifera, and/or red algae (Fig. 9A). Some of the dolostone lithoclasts are coated with black, Mn-rich laminated crusts that are up to 1 cm thick (Figs. 3G, 9A). Each lamina, up to 0.5 mm thick, mimics the morphology of the host lithoclast.

The white limestone lithoclasts include skeletal packstones to grainstones and oncoid grainstones. The skeletal packstone to grainstone lithoclasts, up to 10 cm long and 4 cm wide, include biofragments derived from corals, foraminiferas, and bivalves (Fig. 9B). All of these biofragments have been leached and then filled with calcite cement. The oncoid grainstone lithoclasts, 2 to 5 mm long, are formed of spherical to subspherical terrestrial oncoids (up to 0.5 mm in diameter) that are each characterized by a nucleus and a vaguely laminated cortex. SEM and EDX analyses show that the oncoids are largely formed of micrite, along with trace amount of clay minerals, Mn, and Fe. The black to dark grey limestone lithoclasts (Fig. 3D) are divided into skeletal packstones to grainstones and mudstone. The skeletal packstone to grainstone lithoclasts, up to 3 cm long and 2 cm wide, contain biofragments up to 1.5 cm long derived from corals, foraminifera, and bivalves that have all been leached and then cemented by calcite (Fig. 9C). The grey/black mudstone lithoclasts, which are up to 8 cm long and 4 cm wide, contain scattered gastropods and bivalves (Fig. 9D). In most breccias, these grey/black limestone lithoclasts are intermixed with the skeletal white limestone lithoclasts (Fig. 3D). Besides the obvious difference in colour, the skeletal white lithoclasts are generally larger and more rounded than the grey/black lithoclasts.

The matrices in the breccias are formed of white, red, or orange limestone. The white limestone is divided into skeletal packstones to grainstones and oncoid grainstones. Biofragments in the skeletal white limestones were derived from red algae, foraminifera, corals, bivalves, gastropods, and echinoids (Fig. 9E). The biofragments, up 2 mm long and 1.5 mm wide, are typically encased by a micrite envelope (Fig. 9E). The red algae, foraminifera, and echinoids are commonly well preserved with many of the bivalves and gastropods still being formed of aragonite. In matrices formed of white oncoid grainstones, the spherical to subspherical terrestrial oncoids are 0.2 to 3 mm in diameter, with some having leached foraminifera or shell fragments as their nucleus (Fig. 9F). Based on SEM and EDX analyses, the vaguely laminated cortices are formed of micrite along with trace amount of clay minerals, Mn, and Fe. The surfaces of these oncoids are smooth or crenulated.

In previous studies (Jones and Smith, 1988; Jones, 1992b) the orange and red limestones, were called “lithified terra rossa” because they had the appearance of “soil” and were akin to the terra rossa that is found in many modern sinkholes on the island (Fig. 3H). XRD analysis of these rocks showed, however, that they are formed largely of calcite (> 98%) and only minor amounts of dolomite, quartz, and feldspars. No clay minerals were detected by XRD analysis. Thus, they are herein defined as limestone rather than lithified terra rossa.

The red and orange limestones are petrographically similar with both being formed largely of peloids that are held in spar calcite cement (Fig. 9G, 9H). The sub-spherical to elliptical peloids, 0.1 mm to 1.2 cm in diameter, commonly contain shell fragments derived from bivalves and/or gastropods. Foraminifera are common in the red limestones, whereas aragonitic bivalve fragments and gastropods are common in the orange limestone. Although formed largely of micrite, SEM and EDX analyses show that the peloids also contain minor amounts of clay, dolomite, quartz, and feldspars. The clay, which is probably chorite, is identified based on the bladed morphology of the crystals (< 2 μm long) that are formed of Al, Fe, and Si and trace amounts of K (Figs. 10, 11A, B). Chlorite has also been reported from bauxitic soils found on the Cayman Islands (Ahmad and Jones, 1969). SEM and EDX analyses indicate that (1) the red limestone typically contains more chlorite than the orange limestone, (2) the clay crystals in the red limestone (Fig. 10D) seem to be larger (up to 2 μm) than those in orange limestone (up to 1 μm) (Fig. 10B), (3) quartz and feldspar are more common in the red limestones than the orange limestones, and (4) the amount of Al is similar to that of Si in the orange limestones (Fig. 11A) but much lower than Si in the red limestones (Fig. 11B).

5.2.3. Speleothemic calcite

Voids (up to 1 cm wide and 3 cm long) or fractures (up to 1.5 cm wide) in the sinkhole-filling deposits are commonly lined or filled with brown speleothemic calcite. Like the flowstone covering the surface of the caves in the Cayman Formation (Smith, 1987; Jones and Smith, 1988), the fibrous calcite is banded. Its precipitation conforms to the shape of the cavity.

In some cases, dolostone lithoclasts are found inside the spelethemic calcite (Jones, 1987; Jones, 1992b).

5.3. Oxygen and carbon stable isotopes

The $\delta^{18}O$ and $\delta^{13}C$ values obtained from the different components of the sinkhole-filling deposits can be framed against the $\delta^{18}O$ and $\delta^{13}C$ trends that are known from the limestones of the Ironshore Formation, the calcareous crusts that formed on the unconformities in the Ironshore Formation, the dolostones from the Cayman Formation, and the limestones and dolostones from the Pedro Castle Formation (Fig. 12).

The negative $\delta^{18}O$ and $\delta^{13}C$ values obtained from the rootcretes, limestone lithoclasts, calcite cement in the host dolostones and dolostone lithoclasts, white limestone matrices, and speleothemic calcite follow the same $\delta^{18}O$-$\delta^{13}C$ trend, which is characterized by a wide range of $\delta^{13}C$ values and a narrow range of $\delta^{18}O$ values (Fig. 12). Compared to limestones from the Ironshore Formation, most samples in this group yielded more negative $\delta^{13}C$ values, ranging from -4.4 to -11.6 ‰. In contrast, the $\delta^{18}O$ values that range from -6.4 to -2.6 ‰, are compatible with those obtained from the limestones in the Ironshore Formation. The $\delta^{18}O$ and $\delta^{13}C$ in the calcite (micrite and microspar) that forms the rootcretes tend to vary between localities. Rootcretes from locality HRQ, for example, have more positive $\delta^{18}O$ (average -3.5 ‰) values than those from locality EEP (average -4.6 ‰) and locality SQW (average -5.4 ‰). The $\delta^{13}C$ values in rootcretes from HRQ (average -8.1 ‰,) are akin to those from SQW (average -9.2 ‰) but are more positive than those from EEP (average -10.5 ‰). Irrespective of location, there does not seem to be any trend in the isotope values from the base to the top of individual rootcrete crusts.

The $\delta^{18}O$ and $\delta^{13}C$ in the skeletal white limestone lithoclasts, the skeletal white limestone matrices, and the oncoid lithoclasts and matrices all fall in the ranges of -5.5 to -3.6 ‰ and -11.3 to -4.4 ‰, respectively. The two types of black limestone lithoclasts yielded similar $\delta^{18}O$ and $\delta^{13}C$ values that fall in the ranges of -5.7 to -4.5 ‰ and -11.1 to -6.5 ‰, respectively. Compatible with speleothemic calcite that lines the voids and fractures in sinkhole-filling deposits, calcite cement in the host dolostones and dolostone lithoclasts yielded $\delta^{18}O$ and variable $\delta^{13}C$ values that varied from -6.2 to -4.1 ‰ and from -11.3 to -4.9 ‰, respectively.

The negative $\delta^{18}O$ and $\delta^{13}C$ values in the red and orange limestone matrices are characterized by variable $\delta^{18}O$ and $\delta^{13}C$ that vary from -5.8 to -0.8 ‰ and -11.4 to -8.4 ‰ (Fig. 12), respectively. The $\delta^{18}O$ values are consistent with those obtained from the limestones of the Ironshore Formation. In contrast, the $\delta^{13}C$ values, which are much lower than those obtained from the limestones of the Ironshore Formation, are compatible with the $\delta^{13}C$ values obtained from the rootcretes.

5.4. Trace elements and REE concentration

Except for Mn and Sr, the highest concentrations of trace elements and REE are in the red and orange limestones, whereas the lowest concentrations are in the host dolostones. Compared to the host dolostone and other sinkhole-filling deposits, the rootcrete contains higher concentrations of Mn but lower concentrations of Sr. In the sinkhole-filling deposits, there is a positive correlation between the Al and REE concentrations ($\sum$REE), between the Fe and $\sum$REE, and between the Mn and $\sum$REE (Fig. 13).

The red and orange limestone matrices have different concentrations of Al and Ca but similar Mn and Fe contents. The red limestone, for example, has higher Al (2533 to 4162 ppm, average 3088 ppm) than the orange limestone (1942 to 2586 ppm, average 2313 ppm). The Ca content of the red limestone (274621 to 322890 ppm, average 299246 ppm), is lower than that in the orange limestone (317138 to 349450 ppm, average 338144 ppm).

The ∑REE+Y in the lithoclasts, white limestone matrices, and speleothemic calcite found in sinkholes ranges from 0.3 to 20.0 ppm (average 8.1 ppm), whereas the ∑REE+Y of the red and orange limestone matrices varies from 21.5 to 77.6 ppm (average 46.1 ppm). The ∑REE+Y of rootcrete, in contrast, varies from 1.2 to 307.1 ppm (average 35.1 ppm).

The PAAS-nomalized REE+Y distribution patterns derived from all types of lithoclasts, white limestone matrices and speleothemic calcite are different from those derived from the rootcrete, and the red and orange limestones. Like the Neogene limestones and dolostones and Pleistocene limestones, all of the lithoclasts, white limestone matrices and speleothic calcite are heavy-REE (HREE) enriched (Fig. 14). Their La/Yb and Sm/Yb ratios vary from 0.2 to 0.7 (average 0.5) and from 0.7 to 1.0 (average 0.8), respectively (Fig. 15). These values are akin to those obtained from the Neogene limestones and dolostones and Pleistocene limestones, which yielded La/Yb ratios of 0.2 to 0.7 (average 0.4) and Sm/Yb ratios of 0.3 to 1.0 (average 0.7).

Rootcretes and the red and orange limestones are less enriched in HREE but relatively more enriched in light-REE (LREE) than other sinkhole-filling deposits, the Neogene limestones and dolostones, and the Pleistocene limestones (Fig. 14). The La/Yb (0.1 to 1.0, average 0.5) and Sm/Yb (0.6 to 1.2, average 0.9) ratios obtained from the rootcrete are similar to those from the red and orange limestones (Fig. 15).

With respect to La/Yb and Sm/Yb ratios, the rootcretes, and the red and orange limestones follow the same trend, which is different to from the trend derived from the Neogene limestones and dolostones and Pleistocene limestones found on the Cayman Islands (Fig. 15). Compared to the latter group, the samples obtained from the rootcretes and the red and orange limestone matrices typically yielded higher Sm/Yb ratios but similar La/Yb. The Sm/Yb and La/Yb ratios in the rootcretes and the red and orange limestone matrices are partly overlap the range of values associated with the Jamaican terra rossa (Fig. 15).

6. Interpretation

6.1. Sequential development of void-filling deposits

The absolute age of the void-filling deposits is difficult to determine because they lack fossils that allow accurate dating and many of the lithologies are unlike any known from the stratigraphic succession exposed on Grand Cayman. Thus, the evolution of the sinkhole deposits can only be evaluated relative to the each other and relative to the surrounding bedrock (Table 1). The presence of dolostone lithoclasts derived from the Cayman Formation and/or the Pedro Castle Formation and the lack of dolomite in the rootcrete, limestone lithoclasts, and limestone matrices indicates that emplacement of these sinkhole-filling deposits postdated the last phase of dolomitization, which took place during the early Pliocene highstand (3.6-5.0 Ma), according to Zhao and Jones (2012, 2013).

Sinkholes, which are common features in areas where the Cayman Formation is exposed, can be open or filled with a variety of deposits (Fig. 3). The contrast between open and filled sinkholes indicates that the development of sinkholes is probably an ongoing process, with some of them now being actively filled by loose dolostone lithoclasts derived from surrounding host dolostones of the Cayman Formation (Fig. 3).

The formation of rootcrete and deposition of the limestone matrices were repeated many times. Rootcrete, for example, is present between the host dolostones and the sinkhole-filling deposit, or between different types of sinkhole-filling deposits (Fig. 5). Similarly, matrices formed of skeletal and oncoid white limestone were deposited at many different times. Some of the white limestone matrices that overlie the host dolostones, for example, were subsequently truncated by rootcrete, whereas other limestones formed after many of the rootcretes (Fig. 5). The poorly consolidated nature of these matrices with their well-preserved aragonitic fossils indicates that they probably formed when the limestones of the Ironshore Formation were being deposited and/or as a result of relatively modern deposition associated with storms (Table 1). The age of the oncoid white limestone matrices is not known and could even be forming today.

Today, loose dolostone lithoclasts found in many of the open sinkholes came from the surrounding Cayman Formation (Fig. 3E). Similarly, most of the white dolostone lithoclasts the lithified breccias probably came from the Cayman Formation (Table 1). It is possible, however, that some could have come from the Pedro Castle Formation (Table 1) that once covered this part of the island.

The black and skeletal white limestone lithoclasts, which are of marine origin, cannot be related to any of bedrock succession that is exposed on the Cayman Islands today. Thus, it seems that these lithoclasts were derived from strata that have since been removed by erosion. This suggestion is feasible given that that the period between deposition of the sediments in the Pedro Castle Formation (early-middle Pliocene) and the initiation of the sedimentation for the Ironshore Formation (500-600 ka) (Jones et al., 1994b; Wignall, 1995; Vézina, 1997; Zhao and Jones, 2013; Liang and Jones, 2014) was characterized by oscillating sea levels (Dowsett and Cronin, 1990; Miller et al., 2005, 2011, 2012; Dwyer and Chandler, 2009; Sosdian and Rosenthal, 2009). Deposition during one of the sea level highstands may have produced limestones that were removed by erosion during subsequent lowstands. Thus, the black and skeletal white limestone lithoclasts may have been derived from sequences that were 3.6 Ma to 500-600 ka old (Table 1).

6.2. Rootcrete

The following features indicate a biological, non-marine origin for the rootcrete.

- The presence of numerous spores and filaments (Alonso-Zarza and Jones, 2007),
- The presence of calcified root cells in some of the rootcrete (Alonso-Zarza and Jones, 2007, their Fig. 5).
- The presence of alveolar-septal structures (Fig. 6E), which are commonly associated with plant roots (Klappa, 1978, 1979; Wright, 1986; Wright et al., 1988; Armenteros and Daley, 1998).
- The variable size of the anhedral to subhedral micrite in rootcrete indicates that precipitation of the carbonate was probably biogenically induced (Alonso-Zarza, 1999).
- The presence of needle fiber calcite (NFC), which has been attributed to physicochemical and biological processes. The inorganic processes would have involved solutions that were supersaturated with respect to $CaCO_3$ (James, 1972; Riche et al., 1982; Jones, 2014), whereas biological processes have generally been attributed to plant root and/or fungal activity (Harrison, 1977; Calvet and Juliá, 1983; Callot et al., 1985a, 1985b; Phillips and Self, 1987).
- The voids in the alveolar-septal structures are commonly filled with peloids. The peloids may be related to roots or the activity of microorganisms that are associated with plant roots (Calvet and Juliá, 1983; Jones and Squair, 1989; Alonso-Zarza, 1999, 2003; Miller and James, 2012).
- The lack of marine fossils.
- The homogenous $\delta^{18}O$ and variable $\delta^{13}C$ of the Cayman rootcretes, which are consistent with meteoric diagenesis in the vadose zone (Meyers and Lohmann, 1985; Lohmann, 1988).

The lack of positive covariance between the $\delta^{18}O$ and $\delta^{13}C$ in the rootcretes indicates that evaporation was not involved in the formation of the rootcretes.

Various features associated with the rootcretes, such as the calcified root cells and alveolar-septal structures indicate that the rootcretes probably formed around the roots when the plants were alive. After the decay of the plants, the rootcrete remains with the crust following the outline the cavity that developed while the plants were alive. The rootcrete forms an impermeable barrier that would have impeded fluid draining from the surface, including rainfall and acids produced by the plants, which is similar to the situation associated with rhizogenic calcrete horizons (Goudie, 1983; Reimann and de Caritat, 1998).

Laminar calcrete, which forms in the soil profile under biogenic control of plant roots and their associated microorganisms (Klappa, 1980; Wright et al., 1988, 1995; Alonso-Zarza, 1999), develops through in situ alteration of the host rock (e.g., James, 1972; Goudie, 1973; Arakel, 1982) and/or accretionary build-up (e.g. Wright et al., 1988, 1995; Li and Jones, 2014). For rootcrete, the in situ alteration model is discounted because the rootcrete is formed largely of calcite, whereas the host rock is formed of dolostone. As noted by Alonso-Zarza and Jones (2007), the accretion model is more feasible given that the various microorganisms contribute to the rootcrete formation by (1) binding detrital micrite onto the substrate, (2) acting as nuclei for calcite precipitation, and (3) modifying the local microenviroment so that micrite can be precipitated. Minor amounts of chlorite, feldspar, quartz, and zeolites, which were probably of detrital origin, became incorporated into the rootcrete during these accretionary processes. The incorporation of these minerals are probably responsible for the large variations in the ∑REE+Y, the correlations between ∑REE and Fe, Mn, and Al, the HREE-enriched REE+Y patterns, and the La/Yb and Sm/Yb values that are different from the Cenozoic carbonates found on the

Cayman Islands (Figs. 13-15). The Mn found in the rootcrete is probably related to biological activity (Jones, 1992a).

6.3. Breccia

6.3.1. Lithoclasts

The white dolostone lithoclasts, with their fossil-mouldic porosity, are comparable with the dolostones found in the Cayman Formation and the Pedro Castle Formation. This suggestion is further supported by (1) the stable isotopes from the dolomite that follows the same $\delta^{18}O$-$\delta^{13}C$ trend as the dolostones from these formations (Fig. 12), and (2) REE+Y patterns and La/Yb and Sm/Yb ratios that are akin to those in the dolostones from these formations (Figs. 14, 15). Most of these lithoclasts seem to have been derived from the Cayman Formation.

The composition and microfabrics of the Mn-rich coatings found around some of the dolostone lithoclasts is identical to the Mn-rich coatings evident in the rootcretes, suggesting that their formation was also related to root activity.

The skeletal white and black skeletal limestone lithoclasts, which contain numerous fossils (e.g., corals, foraminifera), are clearly of marine origin. The black mudstone lithoclasts are probably also of marine origin because (1) some lithoclasts are formed of intercalated mudstone and skeletal limestone (Fig. 9D), and (2) the REE+Y signatures of the mudstones are similar to those obtained from the skeletal limestone lithoclasts. This is contrary to opinion of Jones (1992b) who suggested that the black mudstone may have originated in fresh- to brackish-water ponds. The black and skeletal white limestone lithoclasts are intermixed with each other, indicating that they probably originated from contemporary limestone deposits. There are, however, no counterparts to these lithologies in the bedrock succession that is now exposed on

Grand Cayman. The limestones layers from which these lithoclasts came were probably removed by erosion during periods of subaerial exposure.

The black color of carbonate lithoclasts has been attributed to (1) impregnation by Fe or Mn sulphides (Sugden, 1966; Maiklem, 1967; Wright, 1986), (2) forest fires (Barthel, 1974; Strasser, 1984; Shinn and Lidz, 1988), or (3) dissolved, colloidal or very finely particulate organic matter that formed under pedogenic conditions, including organic rich tidal and lacustrine environments, microbial communities, and decayed terrestrial plants (Ward et al., 1970; Folk et al., 1973; Strasser and Davaud, 1983; Strasser, 1984; Leinfelder, 1987; Lang and Tucci, 1997, Miller et al., 2013). On the Cayman Islands, discoloration due to Fe and Mn impregnation seems unlikely because no pyrite was found in the crusts and the Fe and Mn contents are similar to those of white host dolostones. Blackening of carbonates by forest fires requires temperatures between 400 and 500°C (Shinn and Lidz, 1988; Vera and de Cisneros, 1993). Although possible for the Cayman lithoclasts, there is no direct evidence to support this possibility because large forest fires are rare on Grand Cayman and any that do occur are of short duration.

The pedogenic-meteoric diagenetic model seems to be the most feasible explanation for the black limestone lithoclasts found on the Cayman Islands. The lack of black limestone lithoclasts in the sinkholes without rootcrete implies that the environment that favored rootcrete development also favored the development of black limestone lithoclasts. The development of rootcrete is associated with decaying terrestrial plants, which favors organic staining of limestones (Krumbein and Garrels, 1952; Suess, 1970; Strasser and Davaud, 1983; Strasser, 1984; Leinfelder, 1987; Lang and Tucci, 1997; Miller et al., 2013). Organic matter, however, did not blacken all of the lithoclasts in the sinkholes as many of skeletal white limestone lithoclasts remained white. Hips et al. (2011) suggested that blackening by organic matter is related to the presence of unstable minerals (e.g., aragonite and high-Mg calcite). This is because the replacement of unstable minerals would provide the opportunity for the absorption of organic matter into the crystal (Hips et al., 2011). If it is assumed that the blackening processes are linked to the diagenetic alteration of unstable minerals, then the white limestone lithoclasts must have stabilization prior to the onset of the diagenetic processes responsible for the blackening of the lithoclasts. This notion is supported by (1) the fact that some white spots are still evident inside some of the black lithoclasts, and (2) the $\delta^{13}C$ values of the black limestone lithoclasts are more negative than those from the white limestone lithoclasts.

The terrestrial oncoids in the oncoid white limestone lithoclasts and oncoid matrices are consistent with those described by Jones (1991). The subtle variations of the composition of oncoids suggest subtle changes in fine-grained detritus and the ground water (Jones, 1991).

6.3.2. Matrices

The marine fossils and REE signatures indicate that the skeletal white limestone matrices are of marine origin. The presence of aragonitic fossils suggests that these limestone matrices probably formed during or after the Pleistocene (Table 1). Given that these limestones have experienced meteoric diagenesis, which is similar to the limestones from the Ironshore Formation, the different $\delta^{18}O$-$\delta^{13}C$ trend for these white limestone matrices and the limestones from the Ironshore Formation indicates that they probably formed at different times (Fig. 12).

A terrestrial origin for the oncoid white limestone matrices is suggested by (1) the morphological and compositional similarity between these terrestrial oncoids and those described by Jones (1991), and (2) their negative $\delta^{18}O$ and $\delta^{13}C$ values, which are consistent with meteoric diagenesis in the vadose zone (Meyers and Lohmann, 1985; Lohmann, 1988). Jones (1991) suggested that terrestrial oncoids were of biogenic origin. Thus, the environment around rootcretes would be ideal for their development.

The red and orange limestone matrices do not appear to be of marine origin because they are characterized by trace amounts of chlorite, quartz and feldspar crystals, and have different isotopic compositions and REE signatures than the limestones from the Ironshore Formation. The different colours are probably related to variations in the carbonate content and the amount of detrital quartz, feldspar, and chlorite (cf., Porter, 2000; Sun et al., 2011). The quartz, feldspar, and chlorite were probably derived from airborne dust, as on other Caribbean Islands (e.g., Muhs et al., 1990, 2007; Foos, 1991; Borg and Banner, 1996; Herwitz and Muhs, 1995; Muhs, 2001; Muhs and Budahn, 2009). The variable $\delta^{18}O$ and homogenous $\delta^{13}C$ values of the red and orange limestone matrices are consistent with the $\delta^{18}O$-$\delta^{13}C$ trend that is typically associated with evaporation (Salomons et al., 1978; Rossinsky and Swart, 1993). This suggests that the red and orange limestone matrices may have been the product of in situ precipitation that was driven by evaporation.

The $\sum$REE+Y, the La/Yb ratios, and the Sm/Yb ratios from the red and orange limestones are different from those obtained from the Cayman Formation, the Pedro Castle Formation, and the Ironshore Formation (Figs. 14, 15), indicating that REE from authigenic minerals (e.g., Fe- and Mn-oxides) and/or terrigenous sediment (e.g., Nothdurft et al., 2004) are probably involved. For the red and orange limestone matrices, however, the poor correlation between $\sum$REE and Fe, between $\sum$REE and Mn, and between $\sum$REE and Al (Fig. 13), indicates that there is little contamination from authigenic minerals. Terrigenous contamination could, however, have come from airborne dust and/or terra rossa that is present in some areas of the Cayman Islands (Zhao and Jones, 2013).

6.4. Speleothemic calcite

Stable isotope compositions indicate that the speleothemic calcite that coats the walls of many of the voids in the sinkhole-filling deposits was formed from meteoric water. Such precipitation probably took place at the same time as speleothemic calcite was being precipitated in many of the caves on the Cayman Islands, probably as a result of high rainfall (Jones and Smith, 1988; Jones, 1992b).

7. Discussion

The sinkhole-filling deposits formed during sea-level lowstands while the subaerial unconformities were developing. On the eastern part of Grand Cayman, sinkhole development and filling have been processes since the late Pliocene (~3.6 Ma). As a result, the type of sinkhole-filling deposit varied with time as local conditions changed in accord with sea level and climate conditions.

The stable isotope signatures of the sinkhole-filling deposits are similar to those obtained from the calcrete crusts that are found on some of the unconformity surfaces in the Ironshore Formation (Fig. 12). The $\delta^{18}O$ and $\delta^{13}C$ values for these sinkhole fills, however, are significantly different from those that characterize the limestones from the Ironshore Formation and the dolostones and limestones of the Cayman Formation and Pedro Castle Formation (Fig. 12). Such comparisons support the notion that the sinkhole-filling deposits were subject to significantly different diagenetic regimes that were largely mediated by meteoric waters. Such diagenesis, which is commonly associated with erosional unconformities, is typically characterized by evaporation and/or biological activity that yields $\delta^{18}O$ values from -9 ‰ to 3 ‰ and $\delta^{13}C$ values from -12 ‰ to 4 ‰ (Talma and Netterberg, 1983; McKenzie, 1985; Salomons and Mook, 1986; Alonso-Zarza, 2003; Alonso-Zarza and Arenas, 2004). The isotopic compositions of the

Cayman sinkhole-filling deposits fall within these limits, with the $\delta^{13}C$ values being near the limit of -12 to -13 ‰ known for soil carbonates (Cerling, 1984; Burns et al., 1989; Alonso-Zarza, 1999). Such comparisons also indicate that biogenic factors played an important role in the formation of sinkhole-filling deposits. The rootcrete offers clear evidence of such biogenic processes.

For terrestrial deposits, the rare earth elements La (LREE), Sm (MREE), and Yb (HREE) have commonly been used as indicators of provenance and to compare different deposits (Nakai et al., 1993; Clift et al., 2005; Muhs et al., 2007; Muhs and Budahn, 2009). The La/Yb and Sm/Yb ratios for the sinkhole-filling deposits on Grand Cayman plot along a different trend line than that derived from the Miocene dolostones, the Pliocene limestones and dolostones, and the Pleistocene limestones (Fig. 15). Although plotting along the same trend line as for the Jamaican terra rossa, the Cayman sinkhole-filling deposits and Jamaica terra rossa only partly overlap (Fig. 15). These comparisons further emphasis that the sinkhole-filling deposits evolved in a different manner than the Neogene and Pleistocene marine carbonates.

During periods of subaerial exposure, variations in local climate (e.g., rainfall, temperature, storms) would have had a major impact on the deposits that accumulated in the sinkholes. The formation and accumulation of black limestone lithoclasts, dolostone lithoclasts coated with black, Mn-rich laminae, coated grains, aeolian sediments and rootcretes, for example, probably took place during periods when semi-arid climate prevailed (Wright, 1994; D'Argenio and Mindszenty, 1995; Kosir, 2004; Miller et al., 2012, 2013; Brlek et al., 2013). In contrast, precipitation of the speleothemic calcite required wet climates (Jones, 1992b; Miller et al., 2012). Compared to other sinkhole-filling deposits, the red and orange limestone matrices yielded higher $\delta^{18}O$ values (Fig. 12), indicating that the meteoric water involved in their development had probably undergone more evaporation (cf., Li and Jones, 2014). Storm waves were also important because they commonly transported marine sediments from the shallow, offshore lagoons on land and into the sinkholes (Jones, 1992b; Ng et al., 1992).

Plant roots played an important role in the development of the deposits found in the sinkholes. As with rhizogenic calcrete horizons (Mutler and Hoffmeister, 1968; Klappa, 1980; Jones, 1988; Jones and Ng, 1988; Wright, 1994; Kosir, 2004; Alonso-Zarza and Jones, 2007), the roots (1) accelerated bedrock weathering, (2) penetrated into the substrate and thereby increased porosity and permeability, (3) created fluids supersaturated with respect to $CaCO_3$, (4) acted as centres of calcification, and (5) provided substrates and nutrients for symbiotic microorganisms, which may have enhanced the precipitation of micritic cement, formation of the terrestrial oncoids, and blackening of the limestone lithoclasts.

Roots also played a role in the development of the black limestone lithoclasts, because decayed root material and/or symbiotic microorganisms provides organic matter that acted as a coloring agent (Strasser, 1984). These roots may also have created local concentrations of calcium bicarbonate ions in the pore fluids (Miller et al., 2013), which facilitated adsorption of organic matter onto the calcite crystal surface by the alteration of unstable minerals (i.e. aragonite and high-Mg calcite) and creating alkaline and anoxic microenvironments (Krumbein and Garrels, 1952; Suess, 1970; Strasser, 1984).

Black limestone lithoclasts, like those found on the Cayman Islands, are known from many different geological settings throughout the world (e.g., Ward et al., 1970; Perkins, 1977; Beach and Ginsburg, 1980; Strasser and Davaud, 1983; Strasser, 1984; Shinn and Lidz, 1988; Lang and Tucci, 1997; Hips et al., 2001; Miller et al., 2013). Features common to all settings include (1) the angular shape of the lithoclasts, (2) the variable black coloration, (3) lithoclasts formed of mudstone (micritic) or skeletal wackestones, and (4) the lack of lithological counterparts in the surrounding bedrock succession. Although all of the black limestone lithoclasts formed under pedogenic and meteoric diagenetic conditions, commonly in association with calcrete and root cast, plants have rarely been regarded as a factor in their formation (Miller et al., 2013).

Based on the black limestone lithoclasts found in middle Miocene, late Pliocene and Pleistocene deposits across southern Australia, Miller et al. (2013) argued that these lithoclasts were calcified root cells that trapped organic matter into their cellular structures during calcification. This model, however, contrasts with the widely accepted notion that black limestone lithoclasts are reworked marine and/or lacustrine carbonate (Strasser and Davaud, 1983; Strasser, 1984; Leinfelder, 1987; Lang and Tucci, 1997; Hips et al., 2011). The black limestone lithoclasts in the Cayman examples, for example, are of marine origin and display no evidence of calcified root cells.

Some of the sinkhole-filling sediments contain trace amounts of chlorite, quartz and feldspar that could have been derived from (1) dissolution of the bedrock, (2) terra rossa, and/or (3) airborne dust. Ahmad and Jones (1969) argued that the terra rossa found on the Cayman Islands formed as the carbonate bedrock was dissolved and the insoluble residues accumulated. The dolostones and limestones of the Cayman Formation and Pedro Castle Formation, however, contain little non-carbonate material and no quartz or feldspar crystals have ever been found in them. Thus, it seems unlikely that the quartz and feldspars crystals, the immobile trace elements, (e.g., Th, Cr, Zr, Y), and that REE that are found in the sinkhole-filling deposits originated as residues generated by bedrock dissolution. Given that Grand Cayman is geographically isolated by deep oceanic water, the most probable source for these minerals and elements is from wind-blown material. Saharan dust has been regarded as the major contributor to the terra rossa that is found on islands throughout the Caribbean (e.g., Muhs et al., 1990, 2007; Foos, 1991; Borg and Banner, 1996; Herwitz and Muhs, 1995; Muhs, 2001; Muhs and Budahn, 2009). For the sinkhole-filling deposits on Grand Cayman, such an origin is supported by the fact that REE characteristics of the sinkhole-filling deposits are akin to those found in the terra rossa on Jamaica (Muhs and Budahn, 2009).

8. Conclusions

The sinkhole-filling deposits associated with the unconformity that caps the Cayman Formation provide insights into the processes that have been operative since the late Pliocene (~3.6 Ma). New data from these deposits have led to the following important conclusions.

- The geochemical signatures of the sinkhole-filling deposits are significantly different from those of the limestones and dolostones of Neogene and Pleistocene marine carbonates found on Grand Cayman and Cayman Brac.
- The REE signatures of the sinkhole-filling deposits are different from those of the dolostones and limestones that form the Cayman Formation, the Pedro Castle Formation, and the Ironshore Formation. Such differences may offer a means of "fingerprinting" carbonate deposits and determining if they formed in marine or non-marine settings.
- Although lithoclasts derived from the Cayman Formation are common in the sinkholes, no lithoclasts originating from the Pedro Castle Formation or Ironshore Formation have been found.
- The laminated rootcrete formed through accretionary processes that were mediated largely by plant roots.
- Many of the limestone and dolostone lithoclasts found in the sinkhole-filling deposits have no lithological counterparts in the stratigraphic succession found on the Cayman Islands

today. Presumably, they came from strata that have since been stripped from the surface of the island by erosion.

- The black limestone lithoclasts are reworked carbonates that probably became blackened by organic matter during diagenetic alteration.
- The red and orange limestone matrices found in some of the breccias are formed largely of calcite and contain trace amounts of quartz, feldspar and chlorite that probably came from airborne Saharan dust. The different colours in these matrices reflect different amount of quartz, feldspar and chlorite.

Acknowledgments

We are grateful to the Natural Sciences and Engineering Research Council of Canada, which funded this research (Grant A6090 to Jones); Hendrik van Genderen from The Water Authority of Cayman Islands, who helped collect samples used in this study; The Lands and Survey Department; Diane Caird, who ran the XRD analyses; Dr. K. Muehlenbachs, University of Alberta, who provided the laboratory for the stable isotope analyses; George Braybrook, who took the SEM photomicrographs used in this study; Guangcheng Chen, who ran the ICP-MS analyses, and Dr. Cody Miller, an anonymous journal reviewer, and Dr. J. Knight who critically reviewed an earlier version of this manuscript.

References

Ahmad, N., Jones, R.L., 1969. Occurrence of aluminous lateritic soils (bauxites) in the Bahamas and Cayman Islands. Economic Geology 64, 804-808.

Alonso-Zarza, A.M., 1999. Initial stages of laminar calcrete formation by roots: examples from the Neogene of central Spain. Sedimentary Geology 126, 177-191.

Alonso-Zarza, A.M., 2003. Palaeoenvironmental significance of palustrine carbonates and calcretes in the geological record. Earth-Science Reviews 60, 261-298.

Alonso-Zarza, A.M., Arenas, C., 2004. Cenozoic calcretes from the Teruel Graben, Spain: microstructure, stable isotope geochemistry and environmental significance. Sedimentary Geology 167, 91-108.

Alonso-Zarza, A.M., Jones, B., 2007. Root calcrete formation on Quaternary karstic surfaces of Grand Cayman. Geologica Acta 5, 77-88.

Alonso-Zarza, A.M., Wright, V.P., 2010. Calcretes. In: Alonso-Zarza, A.M., Tanner, L.H. (Eds.), Developments in Sedimentology. Elsevier, Oxford, pp. 225-267.

Arakel, A.V., 1982. Genesis of calcrete in Quaternary soil profiles, Hutt and Leeman Lagoons, Western Australia. Journal of Sedimentary Petrology 52, 109-125.

Armenteros, I., Daley, B., 1998. Pedogenic modification and structure evolution in palustrine facies as exemplified by Bembridge Limestone (late Eocene) of the Isle of Wight, southern England. Sedimentary Geology 119, 275-295.

Arts, A.E., 2000. Sedimentology and stratigraphy of the Pedro Castle Formation, southwest Grand Cayman, British West Indies. Unpublished M.Sc. Thesis, University of Alberta, Canada, 107 pp.

Barthel, K.W., 1974. Black pebbles, fossil and recent, on and near coral islands. Proceedings of 2nd International Coral Reef Symposium 2, 395-399.

Beach, D.K., Ginsburg, R.N., 1980. Facies succession of Pliocene-Pleistocene carbonates, northwestern Great Bahama Bank. American Association of Petroleum Geologists Bulletin 64, 1634-1642.

Boero, V., Premoli, A., Melis, P., Barberis, E., Arduino, E., 1992. Influence of climate on the iron oxide mineralogy of terra rossa. Clays and Clay Minerals 40, 8-13.

Borg, L.E., Banner, J.L., 1996. Neodymium and strontium isotopic constraints on soil sources in Barbados, West Indies. Geochimica et Cosmochimica Acta 60, 4193-4206.

Brlek, M., Korbar, T., Košir, A., Glumac, B., Grizelj, A., Otoničar, B., 2013. Discontinuity surfaces in Upper Cretaceous to Paleogene carbonates of central Dalmatia (Croatia): Glossifungites ichnofacies, biogenic calcretes, and stratigraphic implications. Facies 60, 467-487.

Bronger, A., Bruhn-Lobin, N., 1997. Paleopedology of terrae rossae - Rhodoxeralfs from Quaternary calcarenites in NW Morocco. Catena 28, 279-295.

Burns, S., Rossinsky, V., Humphrey, J., 1989. Late Pleistocene mixing zone dolomitization, southeastern Barbados, West Indies: discussion and reply. Sedimentology 36, 1135-1142.

Callot, G., Guyon, A., Mousain, D., 1985a. Inter-relations entre aiguilles de calcite et hyphes mycéliens. Agronomie 5, 209-216.

Callot, G., Mousain, D., Plassard, C., 1985b. Concentrations de carbonate de calcium sur les parois des hyphes mycéliens. Agronomie 5, 143-150.

Calvet, F., Juliá, R., 1983. Pisoids in the caliche profiles of Tarragona (NE Spain). In: Peryt, T.M. (Ed.), Coated Grains. Springer, Berlin, pp. 73-79.

Cerling, T.E., 1984. The stable isotope composition of modern soil carbonate and its relationships to climate. Earth and Planetary Science Letters 71, 229-240.

Clift, P.D., Chan, L.H., Blusztajn, J., Layne, G.D., Kastner, M., Kelly, R.K., 2005. Pulsed subduction accretion and tectonic erosion reconstructed since 2.5 Ma from the tephra record offshore Costa Rica. Geochemistry, Geophysics, Geosystems 6, 21pp.

Clari, P.A., Dela Pierre, F., Martire, L., 1995. Discontinuities in carbonate successions; identification, interpretation and classification of some Italian examples. Sedimentary Geology 100, 97-121.

Coyne, M.K., 2003. Transgressive-regressive cycles in the Ironshore Formation, Grand Cayman, British West Indies. Unpublished M.Sc. Thesis, University of Alberta, Canada, 98 pp.

Cramer, H., 1941. Die systematik der Karstdolinen. Neues Jahrbuch für Mineralogie, Geologie und palaontogie 85, 293-382.

D'Argenio, B., Mindszenty, A., 1995. Bauxites and related paleokarst: tectonic and climatic event markers at regional unconformities. Eclogae Geologicae Helvetiae 88, 453-499.

Daugherty, D.R., Boardman, M.R., Metzler, C.V., 1987. Characteristics and origins of joints and sedimentary dikes of the Bahama Islands. In: Curran, H.A. (Ed.), Proceedings of the Third Symposium on the Geology of the Bahamas. CCFL Bahamian Field Station, Fort Lauderdale, Florida, pp. 45-56.

DeMets, C., Wiggins-Grandison, M., 2007. Deformation of Jamaica and motion of the Gonâve microplate from GPS and seismic data. Geophysical Journal International 168, 362-378.

Der, A.J., 2012. Deposition and sea level fluctuations during Miocene times, Grand Cayman, British West Indies. Unpublished M.Sc. Thesis, University of Alberta, Canada, 101 pp.

Dietz, A., Mathews, J., 1969. Scanning electron microscopy of selected members of the *Streptomyces hygroscopicus* group. Applied Microbiology 18, 694-696.

Dietz, A., Mathews, J., 1971. Classification of *Streptomyces* spore surfaces into five groups. Applied Microbiology 21, 527-533.

Doran, E., 1954. Landforms of Grand Cayman Island, British West Indies. Texas Journal of Science VI, 360-377.

Dowsett, H.J., Cronin, T.M., 1990. High eustatic sea level during the middle Pliocene: evidence from the Southeastern U.S. Atlantic Coastal Plain. Geology 18, 435-438.

Durn, G., 2003. Terra rossa in the Mediterranean region: parent materials, composition and origin. Geologia Croatica 56, 83-100.

Durn, G., Hrenovic, J., Sekovanic, L., 2013. Terra rossa as the substrate for biological phosphate removal from wastewater. Clay Minerals 48, 725-738.

Durn, G., Ottner, F., Slovenec, D., 1999. Mineralogical and geochemical indicators of the polygenetic nature of terra rossa in Istria, Croatia. Geoderma 91, 125-150.

Durn G., Slovenec D., Čović M., 2001. Distribution of iron and manganese in terra rossa from Istria and its genetic implications. Geologia Croatica 54, 27-36.

Dwyer, G.S., Chandler, M.A., 2009. Mid-Pliocene sea level and continental ice volume based on coupled benthic Mg/Ca palaeotemperatures and oxygen isotopes. Philosophical Transactions of the Royal Society A-Mathematical Physical and Engineering Sciences 367, 157-168.

Esteban, M., Klappa, C.F., 1983. Subaerial exposure environments. In: Scholle, P.A., Bebout, D.G., Moore, C.H. (Eds.), Carbonate Depositional Environments. American Association of Petroleum Geologists Memoir 33, pp. 1-96.

Folk, R.L., 1974. The natural history of crystalline calcium carbonate: effect of magnesium content and salinity. Journal of Sedimentary Petrology 44, 40-53.

Folk, R.L., Roberts, H.H., Moore, C.H., 1973. Black phytokarst from Hell, Cayman Islands, British West Indies. Geological Society of America Bulletin 84, 2351-2360.

Foos, A.M., 1991. Aluminous lateritic soils, Eleuthera, Bahamas: A modern analog to carbonate paleosols. Journal of Sedimentary Petrology 61, 340-348.

Ford, D., 1988. Characteristics of dissolution cave systems in carbonate rocks. In: James, N.P., Choquette, P.W. (Eds.), Paleokarst. Springer-Verlag, New York, pp. 25-57.

Ford, D., Williams, P.W., 2007. Karst Hydrogeology and Geomorphology. Wiley, 562 pp.

Garcia-Gonzalez, M.T., Recio, P., 1988. Geochemistry and mineralogy of the clay fraction from some Spanish terra rossa. Agrochimica 32, 161-170.

Goudie, A.S., 1973. Duricrusts in Tropical and Subtropical Landscapes. Claredon, Oxford, 174 pp.

Goudie, A.S., 1983. Calcrete. In: Goudie, A.S., Pye, K. (Eds.), Chemical Sediments and Geomorphology: Precipitates and Residua in the Near-surface Environment. Academic Press, New York, pp. 93-131.

Harrison, R.S., 1977. Caliches profiles: indicator of near-surface subaerial diagenesis, Barbados West Indies. Bulletin of Canadian Petroleum Geology 25, 123-173.

Herwitz, S.R., Muhs, D.R., 1995. Bermuda solution pipe soils: a geochemical evaluation of eolian parent materials. In: Curran, H.A., White, B. (Eds.), Terrestrial and Shallow Marine Geology of the Bahamas and Bermuda. Geological Society of America Special Paper 300, 311-323.

Hillgärtner, H., 1998. Discontinuity surfaces on a shallow-marine carbonate platform (Berriasian, Valanginian, France and Switzerland). Journal of Sedimentary Research 68, 1093-1108.

Hips, K., Haas, J., Vidó, M., Barna, Z., Jovanović, D., Sudar, M.N., Siklósy, Z., 2011. Selective blackening of bioclasts via mixing-zone aragonite neomorphism in Late Triassic limestone, Zlatibor Mountains, Serbia. Sedimentology 58, 854-877.

James, N.P., 1972. Holocene and Pleistocene calcareous crust (caliche) profiles: criteria for subaerial exposure. Journal of Sedimentary Petrology 42, 817-836.

James, N.P., Choquette, P.W., 1990. Limestones-the meteoric diagenetic environment. In: McIlreath, I.A., Morrow, D.W. (Eds.), Diagenesis. Geological Association of Canada, Ottawa, pp. 35-74.

Jones, B., 1987. The alteration of sparry calcite crystals in a vadose setting, Grand Cayman Island. Canadian Journal of Earth Sciences 24, 2292-2304.

Jones, B., 1988. The influence of plants and micro-organisms on diagenesis in caliche: example from the Pleistocene Ironshore Formation on Cayman Brac, British West Indies. Bulletin of Canadian Petroleum Geology 36, 191-201.

Jones, B., 1991. Genesis of terrestrial oncoids, Cayman Islands, British West Indies. Canadian Journal of Earth Sciences 28, 382-397.

Jones, B., 1992a. Manganese precipitates in the karst terrain of Grand Cayman, British West Indies. Canadian Journal of Earth Sciences 29, 1125-1139.

Jones, B., 1992b. Void-filling deposits in karst terrains of isolated oceanic islands: a case study from Tertiary carbonates of the Cayman Islands. Sedimentology 39, 857-876.

Jones, B., 1992c. Construction of spar calcite crystals around spores. Journal of Sedimentary Petrology 62, 1054-1057.

Jones, B., 1994. Geology of the Cayman Islands. In: Brunt, M.A., Davies, J.E. (Eds.), The Cayman Islands: Natural History and Biogeography. Kluwer, Dordrecht, The Netherlands, pp. 13-49.

Jones, B., 2009. Cave pearls - the integrated product of abiogenic and biogenic processes. Journal of Sedimentary Research 79, 689-710.

Jones, B., 2010a. Speleothems in a wave-cut notch, Cayman Brac, British West Indies: The integrated product of subaerial precipitation, dissolution, and microbes. Sedimentary Geology 232, 15-34.

Jones, B., 2010b. Microbes in caves: agents of calcite corrosion and precipitation. In: Pedley, H.M., Rogerson, M. (Eds.), Tufas and Speleothems: Unravelling the Microbial and Physical Controls. Geological Society of London Special Publication 336, pp. 7-30.

Jones, B., 2011. Biogenicity of terrestrial oncoids formed in soil pockets, Cayman Brac, British West Indies. Sedimentary Geology 236, 95-108.

Jones, B., Hunter, I.G., 1994. Evolution of an isolated carbonate bank during Oligocene, Miocene and Pliocene times, Cayman Brac, British West Indies. Facies 30, 25-50.

Jones, B., Peng, X., 2014. Abiogenic growth of needle-fiber calcite in spring towers at Shiqiang, Yunnan Province, China. Journal of Sedimentary Research 84, in press.

Jones, B., Hunter, I.G., Kyser, T.K., 1994a. Revised stratigraphic nomenclature for Tertiary strata of the Cayman Islands, British West Indies. Caribbean Journal of Science 30, 53-68.

Jones, B., Hunter, I.G., Kyser, T.K., 1994b. Stratigraphy of the Bluff Formation (Miocene-Pliocene) and the newly defined Brac Formation (Oligocene), Cayman Brac, British West Indies. Caribbean Journal of Science 30, 30-51.

Jones, B., Luth, R.W., 2002. Dolostones from Grand Cayman, British West Indies. Journal of Sedimentary Research 72, 559-569.

Jones, B., Luth, R.W., 2003. Temporal evolution of Tertiary dolostones on Grand Cayman as determined by $^{87}Sr/^{86}Sr$. Journal of Sedimentary Research 73, 187-205.

Jones, B., Ng, K., 1988. The structure and diagenesis of rhizoliths from Cayman Brac, British West Indies. Journal of Sedimentary Petrology 58, 457-467.

Jones, B., Smith, D.S., 1988. Open and filled karst features on the Cayman Islands: implications for the recognition of paleokarst. Canadian Journal of Earth Sciences 25, 1277-1291.

Jones, B., Squair, C.A., 1989. Formation of peloids in plant rootlets, Grand Cayman, British West Indies. Journal of Sedimentary Petrology 59, 457-467.

Klappa, C.F., 1978. Biolithogenesis of Microcodium: elucidation. Sedimentology 25, 489-522.

Klappa, C.F., 1979. Calcified filaments in Quaternary calcretes: organo-mineral interactions in the subaerial vadose environment. Journal of Sedimentary Petrology 49, 955-968.

Klappa, C.F., 1980. Rhizoliths in terrestrial carbonates: classification, recognition, genesis and significance. Sedimentology 27, 613-629.

Kosir, A., 2004. Microcodium revisited: root calcification products of terrestrial plants on carbonate-rich substrates. Journal of Sedimentary Research 74, 845-857.

Krumbein, W.C., Garrels, R.M., 1952. Origin and classification of chemical sediments in terms of pH and oxidation-reduction potentials. Journal of Geology 60, 1-33.

Kubiëna, W.L., 1953. The soils of Europe. Thomas Murray and Company, London, 104 pp.

Lang, R.A., Tucci, P., 1997. A preliminary study of the causes of the blackening of pebbles in the Cenomanian “breccia with black pebbles” of Camporosello (Lepini Mountains, Italy). Geologica Romana 33, 89-97.

Leinfelder, R.R., 1987. Formation and significance of black pebbles from the Ota Limestone (Upper Jurassic, Portugal). Facies 17, 159-170.

Li, R., Jones, B., 2013. Heterogeneous diagenetic patterns in the Pleistocene Ironshore Formation of Grand Cayman, British West Indies. Sedimentary Geology 294, 251-265.

Li, R., Jones, B., 2014. Calcareous crusts on exposed Pleistocene limestones: a case study from Grand Cayman, British West Indies. Sedimentary Geology 299, 88-105.

Liang, T., Jones, B., 2014. Deciphering the impact of sea-level changes and tectonic movement on erosional sequence boundaries in carbonate successions: a case study from Tertiary strata on Grand Cayman and Cayman Brac, British West Indies. Sedimentary Geology 305, 17-34.

Lohmann, K.C., 1988. Geochemical patterns of meteoric diagenesis system and their application to studies of paleokarst. In: James, N.P., Choquette, P.W. (Eds.), Paleokarst. Springer-Verlag, New York, pp. 58-80.

MacDonald, K.C., Holcombe, T.L., 1978. Inversion of magnetic anomalies and sea-floor spreading in the Cayman Trough. Earth and Planetary Science Letters 40, 407-414.

Macleod, D.A., 1980. The origin of the red Mediterranean soils in Epirus, Greece. Journal of Soil Science 31, 125-136.

MacNeil, A., 2001. Sedimentology, diagenesis, and dolomitization of the Pedro Castle Formation on the Cayman Brac, British West Indies. Unpublished M.Sc. Thesis, University of Alberta, Canada, 128 pp.

MacNeil, A., Jones, B., 2003. Dolomitization of the Pedro Castle Formation (Pliocene), Cayman Brac, British West Indies. Sedimentary Geology 162, 219-238.

Maiklem, W.R., 1967. Black and brown speckled foraminiferal sand from the southern part of the Great Barrier Reef. Journal of Sedimentary Petrology 37, 1023-1030.

Matley, C.A., 1926. The geology of the Cayman Islands (British West Indies) and their relation to the Bartlett Trough. Quarterly Journal of the Geological Society of London 82, 352-387.

McCrea, J.M., 1950. On the isotopic chemistry of carbonates and a paleotemperature scale. The Journal of Chemical Physics 18, 849-857.

McKenzie, J.A., 1985. Carbon isotopes and productivity in the lacustrine and marine environment. In: Stumm, W. (Ed.), Geochemical Processes in Lakes. Wiley, New York, pp. 99-118.

McLennan, S., 1989. Rare earth elements in sedimentary rocks: influence of provenance and sedimentary processes. Reviews in Mineralogy and Geochemistry 21, 169-200.

Meyers, W.J., Lohmann, K.C., 1985. Isotope geochemistry of regionally extensive calcite cement zones and marine components in Mississippian limestones, New Mexico. In: Schneidermann, N., Harris, P.M. (Eds.), Carbonate Cements. Society of Economic Paleontologists and Mineralogists Special Publication 36, pp. 223-239.

Miller, C.R., James, N.P., 2012. Autogenic microbial genesis of middle Miocene palustrine ooids; Nullarbor Plain, Australia. Journal of Sedimentary Research 82, 633-647.

Miller, C.R., James, N.P., Bone, Y., 2012. Prolonged carbonate diagenesis under an evolving late Cenozoic climate: Nullarbor Plain, southern Australia. Sedimentary Geology 261-262, 33-49.

Miller, C.R., James, N.P., Kyser, T.K., 2013. Genesis of blackened limestone clasts at late Cenozoic subaerial exposure surfaces, southern Australia. Journal of Sedimentary Research 83, 339-353.

Miller, K.G., Kominz, M.A., Browning, J.V., Wright, J.D., Mountain, G.S., Katz, M.E., Sugarman, P.J., Cramer, B.S., Christie-Blick, N., Pekar, S.F., 2005. The Phanerozoic record of global sea-level change. Science 310, 1293-1298.

Miller, K.G., Mountain, G.S., Wright, J.D., Browning, J.V., 2011. A 180-million-year record of sea level and ice volume variations from continental margin and deep-sea isotopic records. Oceanography 24, 40-53.

Miller, K.G., Wright, J.D., Browning, J.V., Kulpecz, A., Kominz, M., Naish, T.R., Cramer, B.S., Rosenthal, Y., Peltier, W.R., Sosdian, S., 2012. High tide of the warm Pliocene: implications of global sea level for Antarctic deglaciation. Geology 40, 407-410.

Miyadoh, S., Tsuchizaki, N., Ishikawa, J., Hotta, K., 1997. Digital Atlas of Actinomycetes. Society for Actinomycetes Japan, Akasura Publishing, Tokyo, Japan, 244 pp.

Moresi, M., Mongelli, G., 1988. The relation between the terra rossa and the carbonate-free residue of the underlying limestones and dolostones in Apulia, Italy. Clay Minerals 23, 439-446.

Muhs, D.R., 2001. Evolution of soils on Quaternary reef terraces of Barbados, West Indies. Quaternary Research 56, 66-78.

Muhs, D.R., Budahn, J.R., 2009. Geochemical evidence for African dust and volcanic ash inputs to terra rossa soils on carbonate reef terraces, northern Jamaica, West Indies. Quaternary International 196, 13-35.

Muhs, D.R., Budahn, J., Avila, A., Skipp, G., Freeman, J., Patterson, D., 2010. The role of African dust in the formation of Quaternary soils on Mallorca, Spain and implications for the genesis of Red Mediterranean soils. Quaternary Science Reviews 29, 2518-2543.

Muhs, D.R., Budahn, J., Prospero, J.M., Carey, S.N., 2007. Geochemical evidence for African dust inputs to soils of western Atlantic islands: Barbados, the Bahamas and Florida. Journal of Geophysical Research 112, 1-26.

Muhs, D.R., Bush, C.A., Stewart, K.C., Rowland, T.R., 1990. Geochemical evidence of Saharan dust parent material for soils developed on Quaternary limestones of Caribbean and western Atlantic islands. Quaternary Research 33, 157-177.

Mutler, H.G., Hoffmeister, J.E., 1968. Subaerial laminated crusts of the Florida Keys. Geological Society of America Bulletin 79, 183-192.

Nakai, S, Halliday, A.N., Rea, D.K., 1993. Provenance of dust in the Pacific Ocean. Earth and Planetary Science Letters 119, 143-157.

Ng, K., Jones, B., Beswick, R., 1992. Hydrogeology of Grand Cayman, British West Indies: a karstic dolostone aquifer. Journal of Hydrology 134, 273-295.

Nothdurft, L.D., Webb, G.E., Kamber, B.S., 2004. Rare earth element geochemistry of Late Devonian reefal carbonates, Canning Basin, Western Australia: confirmation of a seawater REE proxy in ancient limestones. Geochimica et Cosmochimica Acta 68, 263-283.

Perfit, M.R., Heezen, B.C., 1978. The geology and evolution of the Cayman Trench. Geological Society of America Bulletin 89, 1155-1174.

Perkins, R.D., 1977. Depositional framework of Pleistocene rocks in south Florida. In: Enos, P., Perkins, R.D. (Eds.), Quaternary sedimentation in south Florida. Geological Society of America Memoir 147, Colorado, pp. 131-198.

Phillips, S.E., Self, P.G., 1987. Morphology, crystallography and origin of needle-fibre calcite in Quaternary pedogenic calcretes of South Australia. Australian Journal of Soil Research 25, 429-444.

Pleydell, S.M., Jones, B., Longstaffe, F.J., Baadsgaard, H., 1990. Dolomitization of the Oligocene-Miocene Bluff Formation on Grand Cayman, British West Indies. Canadian Journal of Earth Sciences 27, 1098-1110.

Porter, S.C., 2000. High-resolution paleoclimatic information from Chinese eolian sediments based on grayscale intensity profiles. Quaternary Research 53, 70-77.

Reid, R.P., MacIntyre, I.G., 1998. Carbonate recrystallization in shallow marine environments: a widespread diagenetic process forming micritized grains. Journal of Sedimentary Research 68, 928-946.

Reimann, C., de Caritat, P., 1998. Chemical Elements in the Environment: Factsheets for the Geochemist and Environmental Scientist. Springer-Verlag, Berlin, 398 pp.

Riche, G., Rambaud, D., Riera, M., 1982. Etude morphologique d'un encroûtement calcaire, Région d'Irecê, Bahia, Brésil. Cahiers Orstom Série Pédologie 19, 257-270.

Rossinsky, V., Swart, P.K., 1993. Influence of climate on the formation and isotopic composition of calcretes. Geophysical Monograph 78, 67-75.

Salomons, W., Goudie, A., Mook, W.G., 1978. Isotopic composition of calcrete deposits from Europe, Africa and India. Earth Surface Processes 3, 43-57.

Salomons, W., Mook, W.G., 1986. Isotope geochemistry of carbonates in the weathering zone. In: Fritz, P., Fontes, J.Ch. (Eds.), Handbook of Environmental Isotope Geochemistry Volume 2. Elsevier, Amsterdam, pp. 239-269.

Sattler, U., Immenhauser, A., Hillgärtner, H., Esteban, M., 2005. Characterization, lateral variability and lateral extent of discontinuity surfaces on a carbonate platform (Barremian to lower Aptian, Oman). Sedimentology 52, 339-361.

Shinn, E.A., Lidz, B.H., 1988. Blackened limestone pebbles: fire at subaerial unconformities. In: James, N.P., Choquette, P.W. (Eds.), Paleokarst. Springer-Verlag, New York, pp 117-131.

Smart, P.L., Palmer, R.J., Whitaker, F., Wright, V.P., 1988. Neptunian dikes and fissure fills: an overview and account of some modern examples. In: James, N.P., Choquette, P.W. (Eds.), Paleokarst. Springer-Verlag, New York, pp. 149-163.

Smith, D.S., 1987. The genesis of speleothemic calcite deposits on Grand Cayman, British West Indies. Unpublished M.Sc. thesis, University of Alberta, Canada, 171 pp.

Sosdian, S., Rosenthal, Y., 2009. Deep-sea temperature and ice volume changes across the Pliocene–Pleistocene climate transitions. Science 325, 306-310.

Stace, H.C.T., 1956. Chemical characteristics of terra rossas and rendzinas of south Australia. Journal of Soil Science 7, 280-293.

Stephens, C.G., 1953. A Manual of Australian Soils. Commonwealth Scientific and Industrial Research Organization, Melbourne, 48 pp.

Strasser, A., 1984. Black-pebble occurrence and genesis in Holocene carbonate sediments (Florida Keys, Bahamas, and Tunisia). Journal of Sedimentary Petrology 54, 1097-1109.

Strasser, A., Davaud, E., 1983. Black pebbles of the Purbeckian (Swiss and French Jura): lithology, geochemistry and origin. Eclogae Geologicae Helvetiae 76, 551-580.

Suess, E., 1970. Interaction of organic compounds with calcium carbonate. Geochimica et Cosmochimica Acta 34, 157-168.

Sugden, W., 1966. Pyrite staining of pellety debris in carbonate sediments from the Middle East and elsewhere. Geological Magazine 103, 250-255.

Sun, Y., He, L., Liang, L., An, Z., 2011. Changing color of Chinese loess: Geochemical constraint and paleoclimatic significance. Journal of Asian Earth Sciences 40, 1131-1138.

Talma, A.S., Netterberg, F., 1983. Stable isotope abundances in calcretes. In: Wilson, R.C.L. (Ed.), Residual Deposits: Surface Related Weathering Processes and Materials. Geology Society of London Special Publication 11, Blackwell Scientific Publications, Oxford, pp. 221-233.

Torrent, J., 1995. Genesis and Properties of the Soils of the Mediterranean Regions. Dipartimento di Scienze Chimico-Agrarie, Universitá degli Studi di Napoli Federico II, 111 pp.

Tresner, H.D., Davies, M.C., Backus, E.J., 1961. Electron microscopy of Streptomycetes spore morphology and its role in species differentiation. Journal of Bacteriology 81, 70-80.

Tucker, M., 1990. Diagenetic processes, products and environments. In: Tucker, M.E., Wright, V.P., Dickson, J.A.D. (Eds.), Carbonate Sedimentology. Blackwell Scientific Publications, Oxford, pp. 314-364.

Vera, J.A., de Cisneros, J., 1993. Palaeogeographic significance of black pebbles (Lower Cretaceous, Prebetic, southern Spain). Palaeogeography, Palaeoclimatology, Palaeoecology 102, 89-102.

Vézina J.V., 1997. Stratigraphy and sedimentology of the Pleistocene Ironshore Formation at Rogers Wreck Point, Grand Cayman: a 400 Ka Record of Sea-level Highstands. Unpublished M.Sc. Thesis, University of Alberta, Canada, 131 pp.

Vézina, J.V., Jones, B., Ford, D.C., 1999. Sea-level highstands over the last 500,000 years: evidence from the Ironshore Formation on Grand Cayman, British West Indies. Journal of Sedimentary Research 69, 317-327.

Ward, W.C., Folk, R.L., Wilson, J.L., 1970. Blackening of eolianite and caliche adjacent to saline lakes, Isla Mujeres, Quintana Roo, Mexico. Journal of Sedimentary Petrology 40, 548-555.

Wignall, B.D., 1995. Sedimentology and diagenesis of the Cayman (Miocene) and Pedro Castle (Pliocene) Formations at Safe Haven, Grand Cayman, British West Indies. Unpublished M.Sc. Thesis, University of Alberta, Canada, 110 pp.

Wright, V.P., 1986. The role of fungal biomineralization in the formation of early Carboniferous soil fabrics. Sedimentology 33, 831-838.

Wright, V.P., 1989. Terrestrial stromatolites and laminar calcretes: a review. Sedimentary Geology 65, 1-13.

Wright, V.P., 1994. Paleosols in shallow marine carbonate sequences. Earth-Science Reviews 35, 367-395.

Wright, V.P., Platt, N.H., Marriot, S.B., Beck, V.H., 1995. A classification of rhizogenic (root-formed) calcretes, with examples from the Upper Jurassic-Lower Carboniferous of Spain and Upper Cretaceous of southern France. Sedimentary Geology 100, 143-158.

Wright, V.P., Platt, N.H., Marriot, S.B., Beck, V.H., 1997. A classification of rhizogenic (root-formed) calcretes, with examples from the Upper Jurassic-Lower Cretaceous of Spain and Upper Cretaceous of southern France-reply. Sedimentary Geology 110, 305-307.

Wright, V.P., Platt, N.H., Wimbledon, W., 1988. Biogenic laminar calcretes: evidence of calcified root mat horizons in paleosols. Sedimentology 35, 603-620.

Zhao, H.W., Jones, B., 2012. Origin of "Island Dolostones": a case study from the Cayman Formation (Miocene), Cayman Brac, British West Indies. Sedimentary Geology 243-244, 191-206.

Zhao, H.W., Jones, B., 2013. Distribution and interpretation of rare earth elements and yttrium in Cenozoic dolostones and limestones on Cayman Brac, British West Indies. Sedimentary Geology 284-285, 26-38.

Figure Captions

Fig. 1. Location and geology of Grand Cayman and Cayman Brac. (A) Location, tectonic and bathymetric setting of the Cayman Islands. Modified from Jones (1994), and based on maps from Perfit and Heezen (1978) and MacDonald and Holcombe (1978). (B) Geology map of Grand Cayman (modified from Jones, 1994) showing localities EEP (East End Pit), HRQ (High Rock Quarry), HMB (Half Moon Bay), and Pedro Castle (PC) where samples were collected. (C) Geology map of Cayman Brac (modified from Jones, 1994) showing locality SQW (Scott Quarry West).

Fig. 2. Stratigraphic succession on Grand Cayman and Cayman Brac (modified from Jones, 1994).

Fig. 3. Field photographs of sinkholes and sinkhole-filling deposits on Grand Cayman and Cayman Brac. Locality codes as for Figure 1. (A) General view of phytokarst surface on Cayman Formation, central part of Cayman Brac. Sinkholes are located between the pinnacles. (B) Open sinkhole in Cayman Formation on Cayman Brac that is at least 16 m deep. (C) Open sinkhole in Cayman Formation on Grand Cayman. Near EEP. (D) Cross-section through sinkhole lined with rootcrete (RC) and filled with breccia (BR). Note lithoclasts of various colours. Locality EEP. (E) Open sinkhole in Cayman Formation with loose dolostone lithoclasts (from Cayman Formation) on floor of sinkhole. Near locality EEP. (F) White dolostone lithoclasts from Cayman Formation with Mn-rich coatings filling sinkhole in Cayman Formation. Locality HRQ. (G) White dolostone lithoclasts held in red limestone matrices; note that some dolostone lithoclasts are coated by black, Mn-rich laminae. Locality HRQ. (H) Contrast between red (left) and orange limestones (right) in Pedro Castle Formation. Locality PC.

Fig. 4. Field photographs of rootcrete lining walls of sinkholes developed in the Cayman Formation. (A) Inner surface of rootcrete lining sinkhole. Arrow indicates location of panel B. Locality HRQ. (B) Rootcrete with Mn-rich laminae coating surface of sinkhole developed in the white dolostones of the Cayman Formation (CF). Locality HRQ. (C) Rootcrete lining wall of sinkhole developed in dolostones of the Cayman Formation (CF). (D) Cut and polished section through rootcrete developed on white dolostone of the Cayman Formation (CF). Locality HRQ.

Fig. 5. Schematic diagram, based on the analysis of numerous sinkholes on Grand Cayman, summarizing the spatial relationships between different sinkhole-filling deposits.

Fig. 6. Thin section microphotographs showing petrographic features of rootcrete. All images with plane polarized light. Locality codes as for Figure 1. (A) Rootcrete overlying host dolostone of the Cayman Formation. Locality HRQ. Yellow square indicates location of panel B. (B) Boundary between host dolostones and rootcrete. Note peloids in the rootcrete. Locality HRQ. (C) Contrast between laminae in rootcrete. Locality HRQ. Yellow square indicates location of panel (D). (D) Mn-rich lamina in rootcrete. Locality HRQ. (E) Alveolar septa structure. Locality EEP. (F) Peloids filling voids between septa in alveolar septa structure. Note spar calcite inside some of the peloids. Locality SQW.

Fig. 7. SEM photomicrogaphs showing micro-fabrics in rootcrete. Locality codes as for Figure 1. Black circles labeled E1 to E5 indicate locations of EDX analyses shown in Figure 8. (A) Spores (S) and reticulate Mn-Fe precipitate (yellow arrow) embedded in micrite in black lamina of rootcrete. Note scattered chlorite plates (blue arrows). Locality SQW. (B) Fuzzy Mn precipitate coating on surfaces of calcite crystals. Locality EEP. (C) Boring (yellow arrow) in the biofragment derived from bivalve. Locality EEP. (D) Zeolite (Z) found in the

red lamina of rootcrete. Locality HRQ. (E) Dolomite (D) rhombs associated with micrite and microspar (C) in red lamina. Locality HRQ. (F) Feldspar (yellow arrow) in red lamina. Locality HRQ. (G) Quartz (Q) in red lamina. Locality HRQ. (H) Chlorite platelets (yellow arrows) arranged perpendicular to the peloid surface, SQW. (I) Collpased filament (yellow arrow) in micrite. Locality SQW. (J) Type I spore, with smooth surface. Opening on top of spore is probably an attachment collar. The surrounding platelets are chlorite. Locality SQW. (K) Type II, smooth spore with radiating spines. Locality SQW. (L) Type III, smooth spores with pores surrounded by low rims, SQW. (M) Type I reticulate filament (yellow arrow) with diamond-shaped openings on surface. Locality SQW. (N) Type II filament (yellow arrow) with isolated spines on surface. Locality SQW. Note fiber calcite crystals associated with the type I and type II filaments. (O) Type III, branching filaments (yellow arrows) that have been completely replaced by euhedral calcite crystals. Locality EEP.

Fig. 8. EDX analyses for various laminae in rootcrete. See Figure 7 for precise locations of each analysis.

Fig. 9. Thin section microphotographs showing petrographic features of breccias in sinkholes. Locality codes as for Figure 1. (A) Coated dolostone lithoclast. Locality HRQ. (B) Skeletal white limestone lithoclasts (above yellow arrows) in the skeletal white limestone matrix (below yellow arrows). Locality EEP. (C) Micro-fabrics in skeletal black limestone lithoclast. Note corals (C) and pseudomorphically replaced foraminifera (F). Locality EEP. (D) Mudstone (right) and interclast packstone (left) in black limestone lithoclast. Locality EEP. (E) Unaltered biofragments, derived largely from red algae (R), in skeletal white limestone matrix. Locality EEP. (F) Oncoid white limestone matrix below rootcrete. Note some oncoid grains have leached biofragments as their nuclei. Locality EEP. (G) Micro-fabrics in orange

limestone matrix showing peloids (black arrows), SQW. (H) Micro-fabrics in red limestone matrices showing peloids (black arrows). Locality EEP.

Fig. 10. SEM photomicrogaphs of micro-fabrics in orange and red limestones. Locality codes as for Figure 1. Black circles labeled E6 and E7 indicate locations of EDX analyses shown in Figure 11. (A) Peloid in orange limestone matrix. Locality EEP. Black square indicates location of panel (B). (B) Chlorite in orange limestone matrix. Locality EEP. (C) Chlorite in red limestone matrices. Locality HRQ. Black square indicates location of panel D. (D) A platy chlorite crystal. Locality HRQ. Note that chlorite in red limestone matrices is finer than that in red limestone matrices.

Fig. 11. EDX analyses for chlorite in red and orange limestones. See Figure 10 for precise locations of each analysis.

Fig. 12. Cross-plot of $\delta^{18}O$ versus $\delta^{13}C$ for sinkhole-filling deposits, Miocene-Pliocene limestones and dolostones.

Fig. 13. Cross plots showing relationship between $\sum$REE of sinkhole-filling deposits and Al (A), Mn (B) and Fe (C).

Fig. 14. PAAS-nomalized REE pattern of carbonates from Cenozoic succession (A) and sinkhole-filling deposits (B and C).

Fig. 15. Cross plot showing the correlation between Sm/Yb versus La/Yb in sinkhole-filling deposits, Jamaican terra rossa, and the carbonate from the Cayman Formation, Pedro Castle Formation and Ironshore Formation on Grand Cayman and Cayman Brac.

Table 1. Sequential development of sinkhole-filling deposits associated with the exposed Cayman Formation

Component	Numbers of episodes	Provenance	Age	Evidence	Active today	Reference
Sinkhole	Multiple		Post late dolomitization		Yes	Jones and Smith, 1988 Jones, 1992b
Rootcrete	Multiple	In situ growth	Post late dolomitization	No dolomite	Probably	Jones, 1992b Alonso-Zarza and Jones, 2007
Dolostone lithoclasts	Numerous and ongoing	Cayman Formation or Pedro Castle Formation	Middle Miocene or Early Pliocene	Same lithologies as in Cayman Formation and Pedro Castle Formation	Yes	Jones, 1992b
Skeletal white and black limestone lithoclasts	Probably one	Unknown marine carbonate	Late Pliocene to Pleistocene	Lithology unlike any bedrock in area	No	Jones and Kahle, 1985 Jones, 1992b
Skeletal white matrices	At least two	Marine skeletal deposits, but not the Ironshore Formation itself	Pleistocene or modern	Well preserved fossils, poorly consolidated	Yes	Jones, 1992b
Oncoid white limestone matrices and lithoclasts	At least two	Terrestrial	Post dolomitization	Terrestrial oncoids cemented by calcite	No	Jones, 1991 Jones, 1992b Jones, 2012
Red and orange limestone matrices	At least two	In situ precipitation, mixed traces of soil	Pleistocene	Aragonitic gastropods and bivalves not leached	No	Ahmed and Jones, 1969 Jones and Smith, 1988 Jones, 1992b

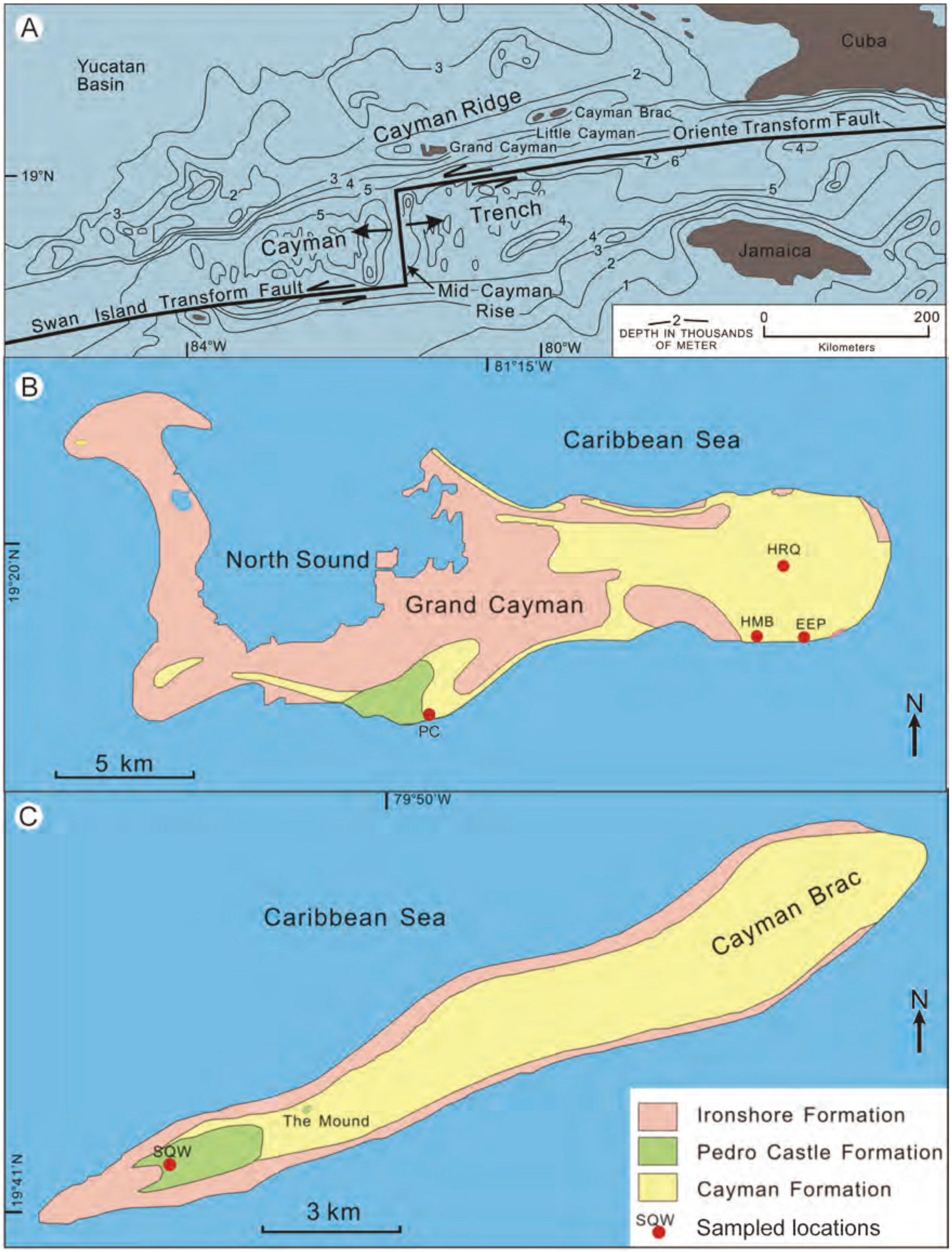
A
Yucatan Basin
Cuba
Cayman Ridge
Cayman Brac
Little Cayman
Grand Cayman
Oriente Transform Fault
19°N
Cayman
Trench
Jamaica
Mid-Cayman Rise
Swan Island Transform Fault
84°W
80°W
DEPTH IN THOUSANDS OF METER
0
200
Kilometers
B
81°15'W
Caribbean Sea
North Sound
Grand Cayman
HRQ
HMB
EEP
PC
19°20'N
5 km
N
C
79°50'W
Caribbean Sea
Cayman Brac
The Mound
SQW
19°41'N
3 km
N
Ironshore Formation
Pedro Castle Formation
Cayman Formation
Sampled locations

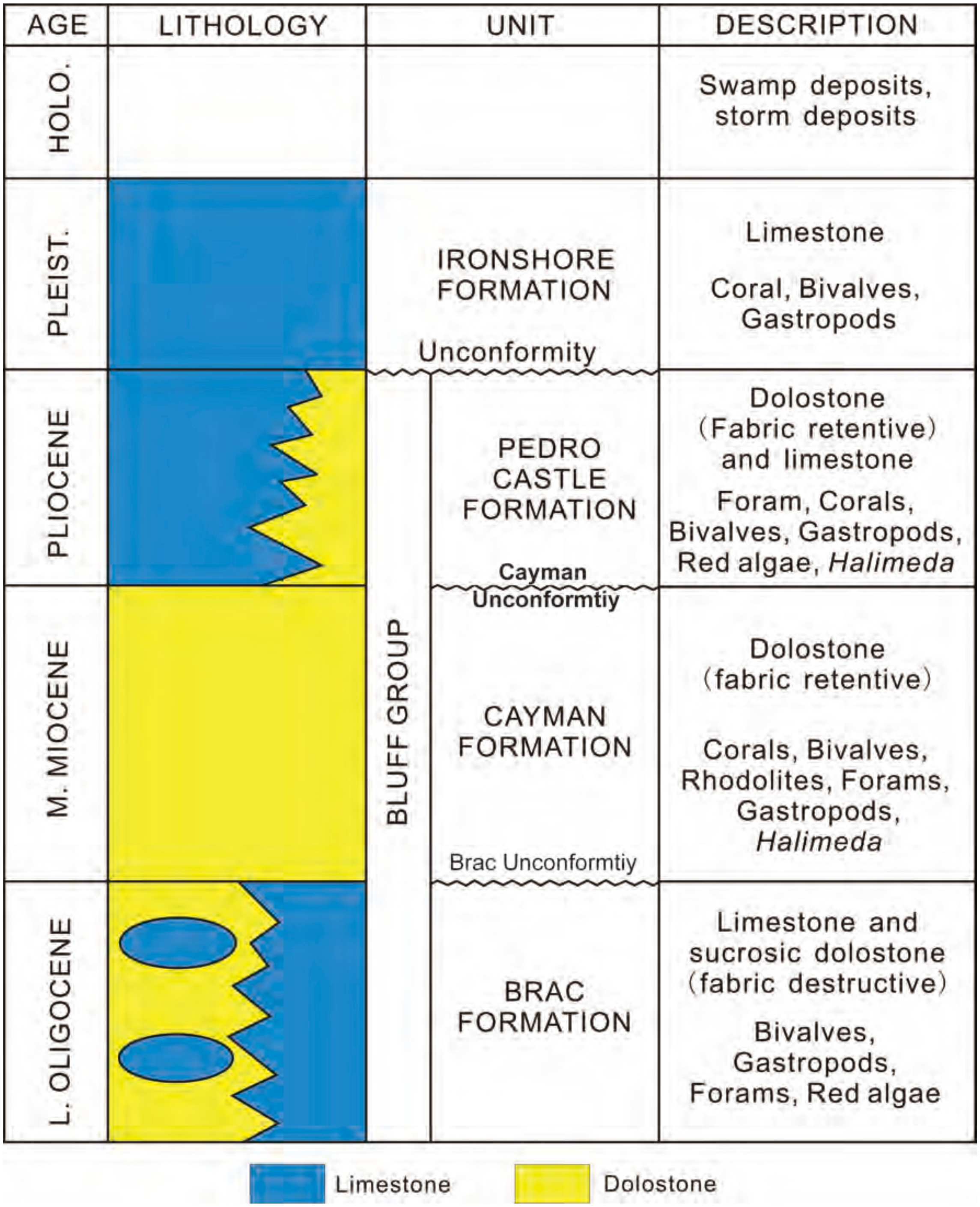
AGE
LITHOLOGY
UNIT
DESCRIPTION
HOLO.
Swamp deposits, storm deposits
PLEIST.
IRONSHORE FORMATION
Unconformity
Limestone
Coral, Bivalves, Gastropods
PLIOCENE
PEDRO CASTLE FORMATION
Cayman Unconformtiy
Dolostone (Fabric retentive) and limestone
Foram, Corals, Bivalves, Gastropods, Red algae, *Halimeda*
M. MIOCENE
BLUFF GROUP
CAYMAN FORMATION
Brac Unconformtiy
Dolostone (fabric retentive)
Corals, Bivalves, Rhodolites, Forams, Gastropods, *Halimeda*
L. OLIGOCENE
BRAC FORMATION
Limestone and sucrosic dolostone (fabric destructive)
Bivalves, Gastropods, Forams, Red algae
Limestone
Dolostone

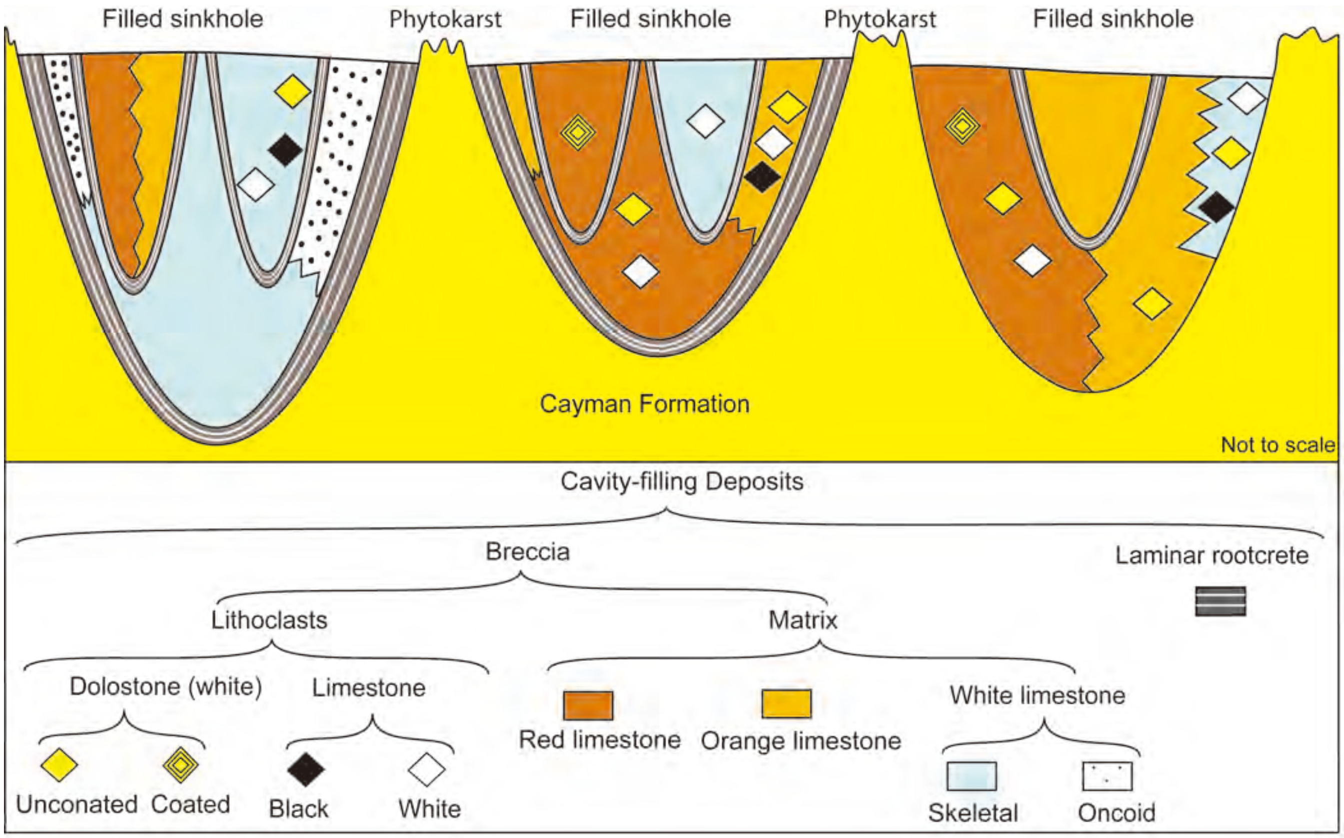

Filled sinkhole
Phytokarst
Filled sinkhole
Phytokarst
Filled sinkhole
Cayman Formation
Not to scale
Cavity-filling Deposits
Breccia
Laminar rootcrete
Lithoclasts
Matrix
Dolostone (white)
Limestone
Unconated
Coated
Black
White
Red limestone
Orange limestone
White limestone
Skeletal
Oncoid

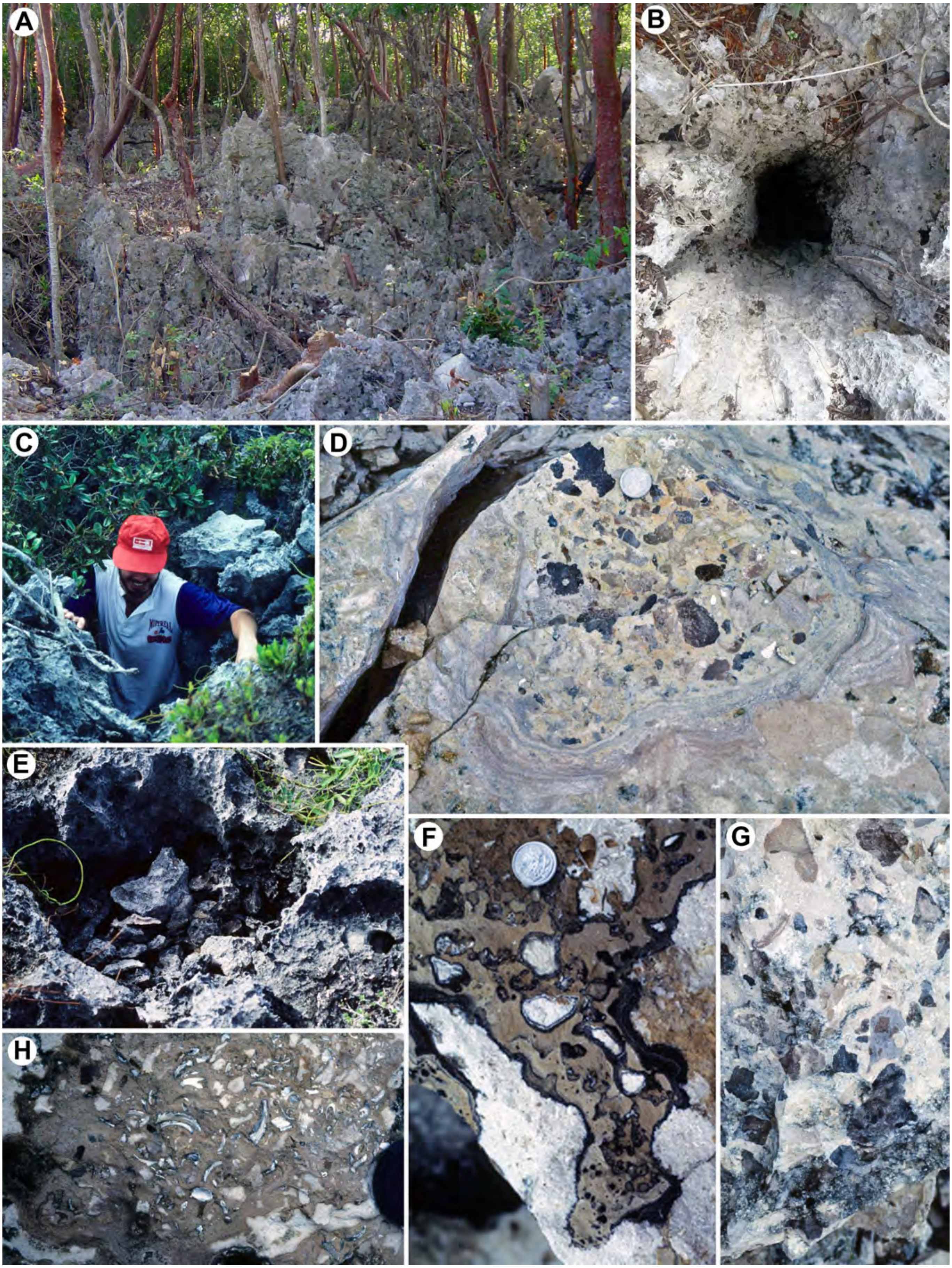
A
B
C
D
E
F
G
H

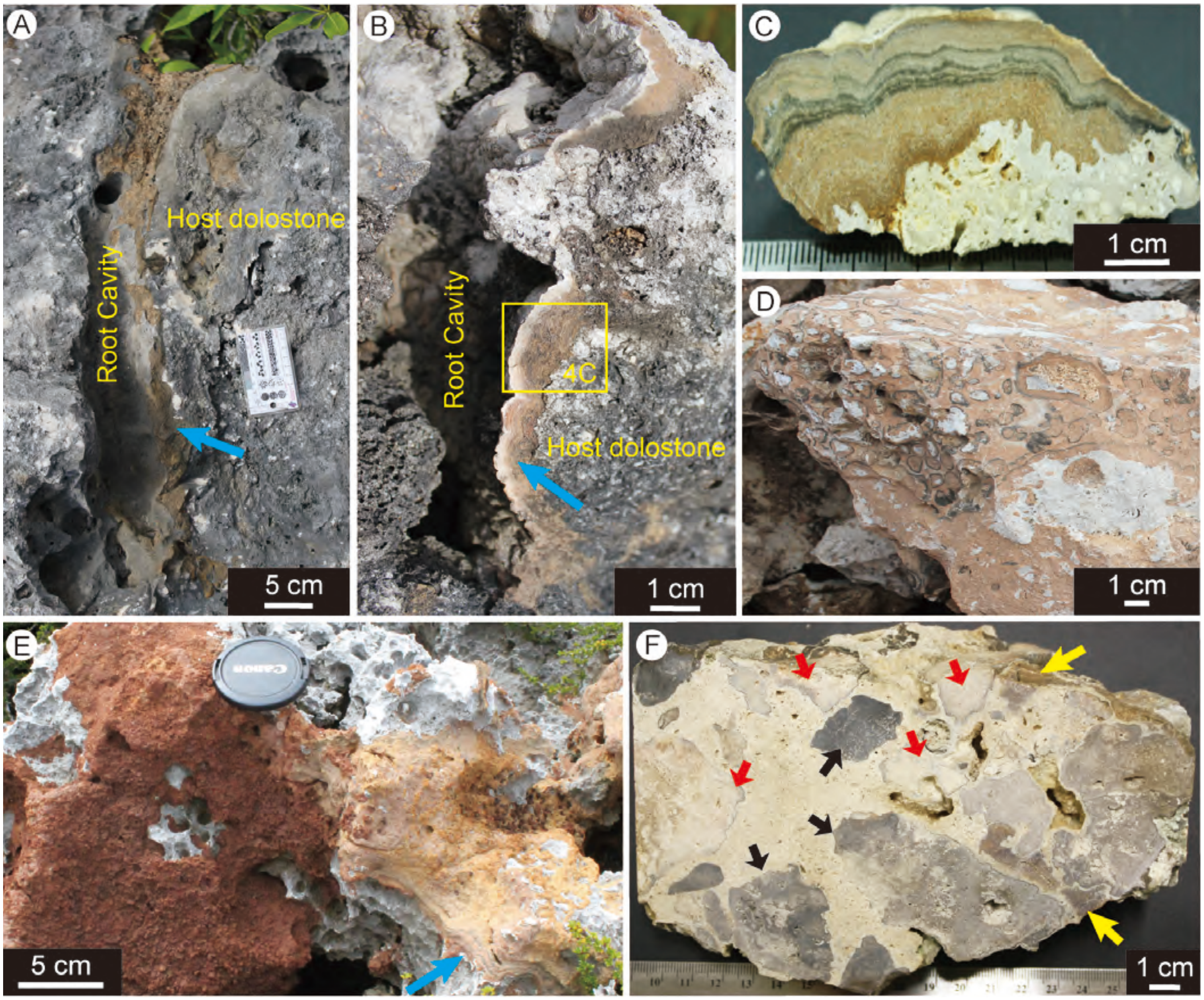
A
Host dolostone
Root Cavity
5 cm
B
Root Cavity
4C
Host dolostone
1 cm
C
1 cm
D
1 cm
E
5 cm
F
1 cm

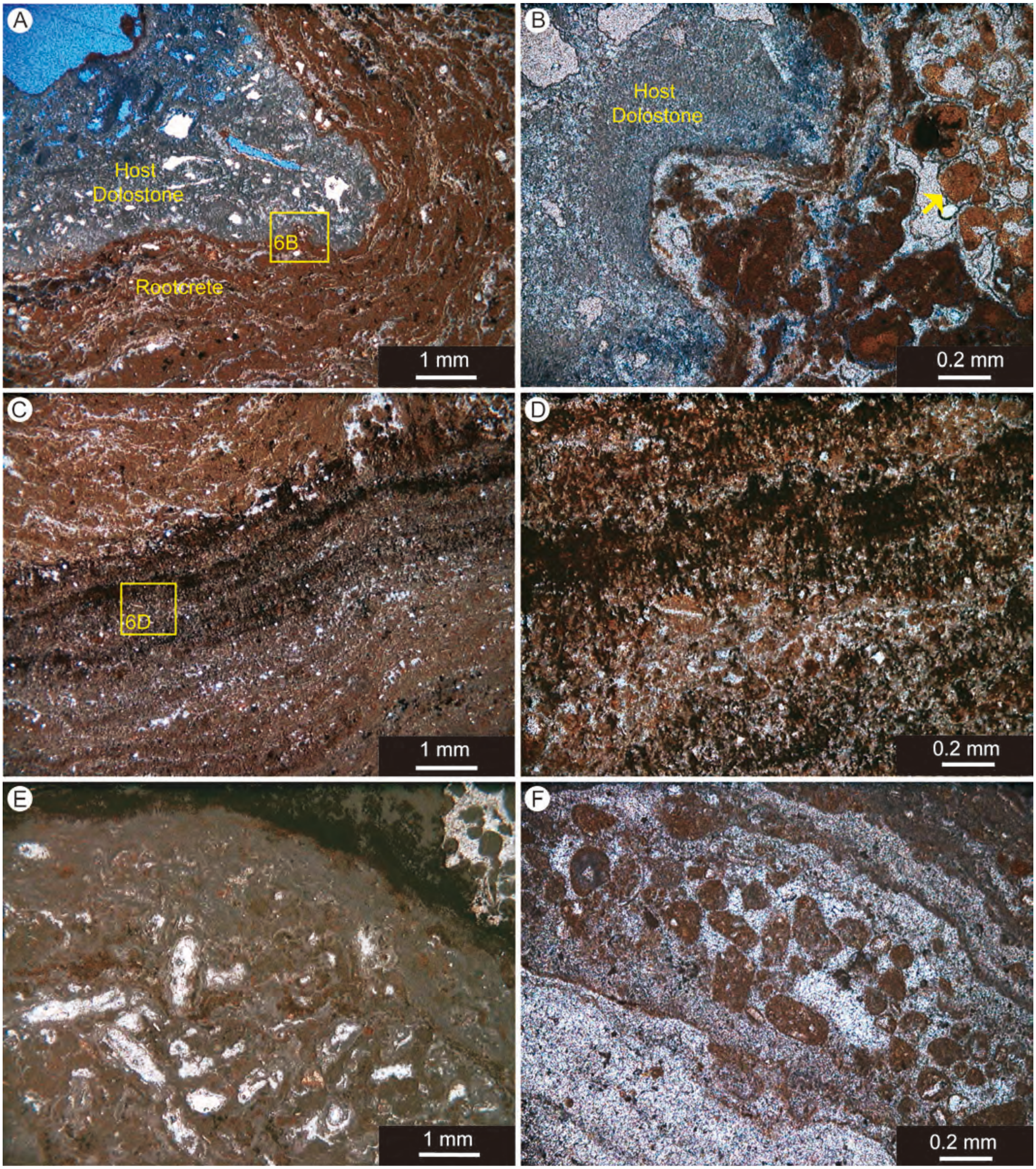
A
Host
Dolostone
6B
Rootcrete
1 mm
B
Host
Dolostone
0.2 mm
C
6D
1 mm
D
0.2 mm
E
1 mm
F
0.2 mm

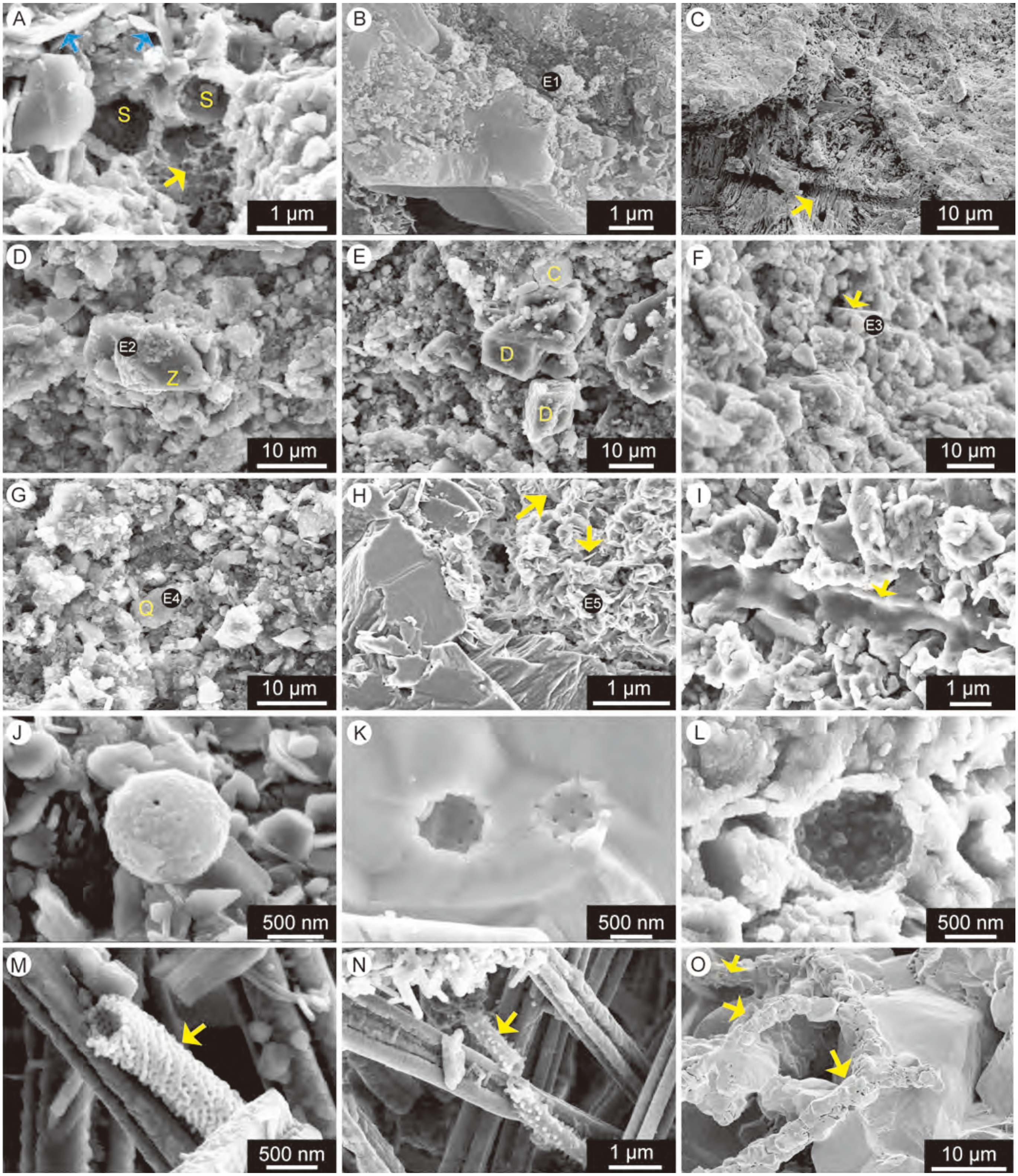
A
S
S
1 µm
B
E1
1 µm
C
10 µm
D
E2
Z
10 µm
E
C
D
D
10 µm
F
E3
10 µm
G
E4
Q
10 µm
H
E5
1 µm
I
1 µm
J
500 nm
K
500 nm
L
500 nm
M
500 nm
N
1 µm
O
10 µm

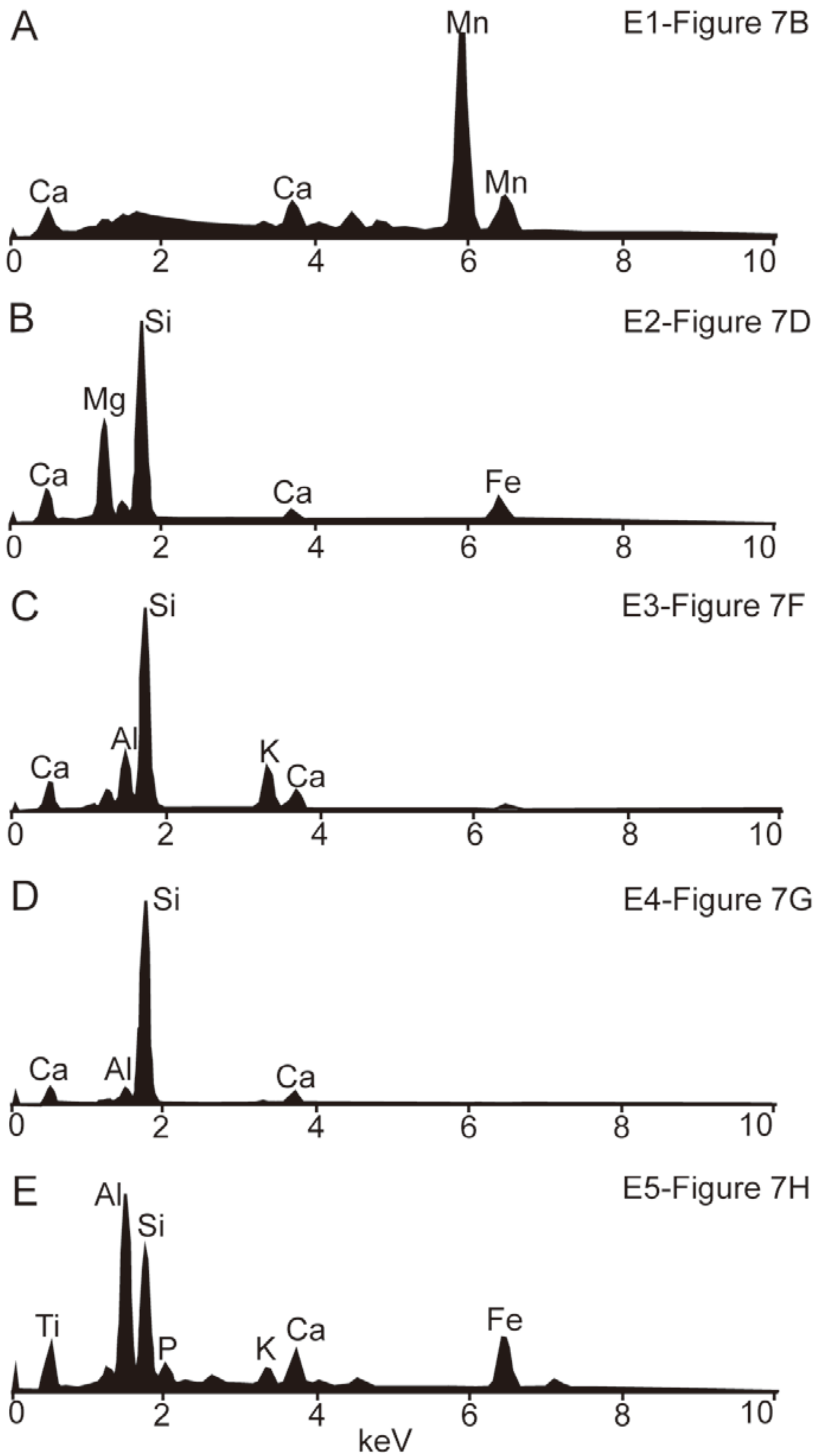

A
E1-Figure 7B
Mn
Ca
Ca
Mn
0
2
4
6
8
10
B
E2-Figure 7D
Si
Mg
Ca
Ca
Fe
0
2
4
6
8
10
C
E3-Figure 7F
Si
Al
Ca
K
Ca
0
2
4
6
8
10
D
E4-Figure 7G
Si
Ca
Al
Ca
0
2
4
6
8
10
E
E5-Figure 7H
Al
Si
Ti
P
K
Ca
Fe
0
2
4
6
8
10
keV

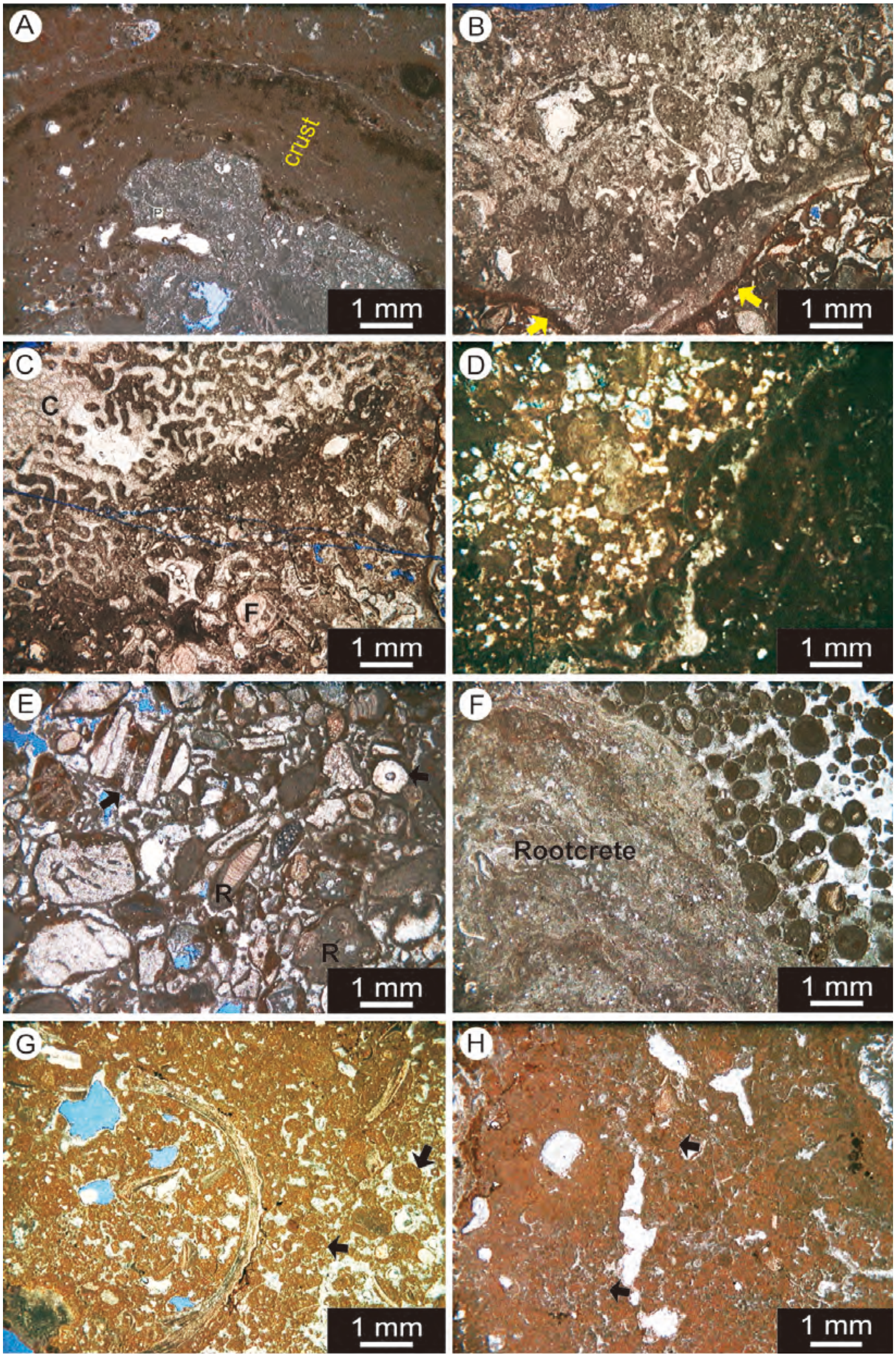
A
crust
1 mm
B
1 mm
C
C
F
1 mm
D
1 mm
E
R
R
1 mm
F
Rootcrete
1 mm
G
1 mm
H
1 mm

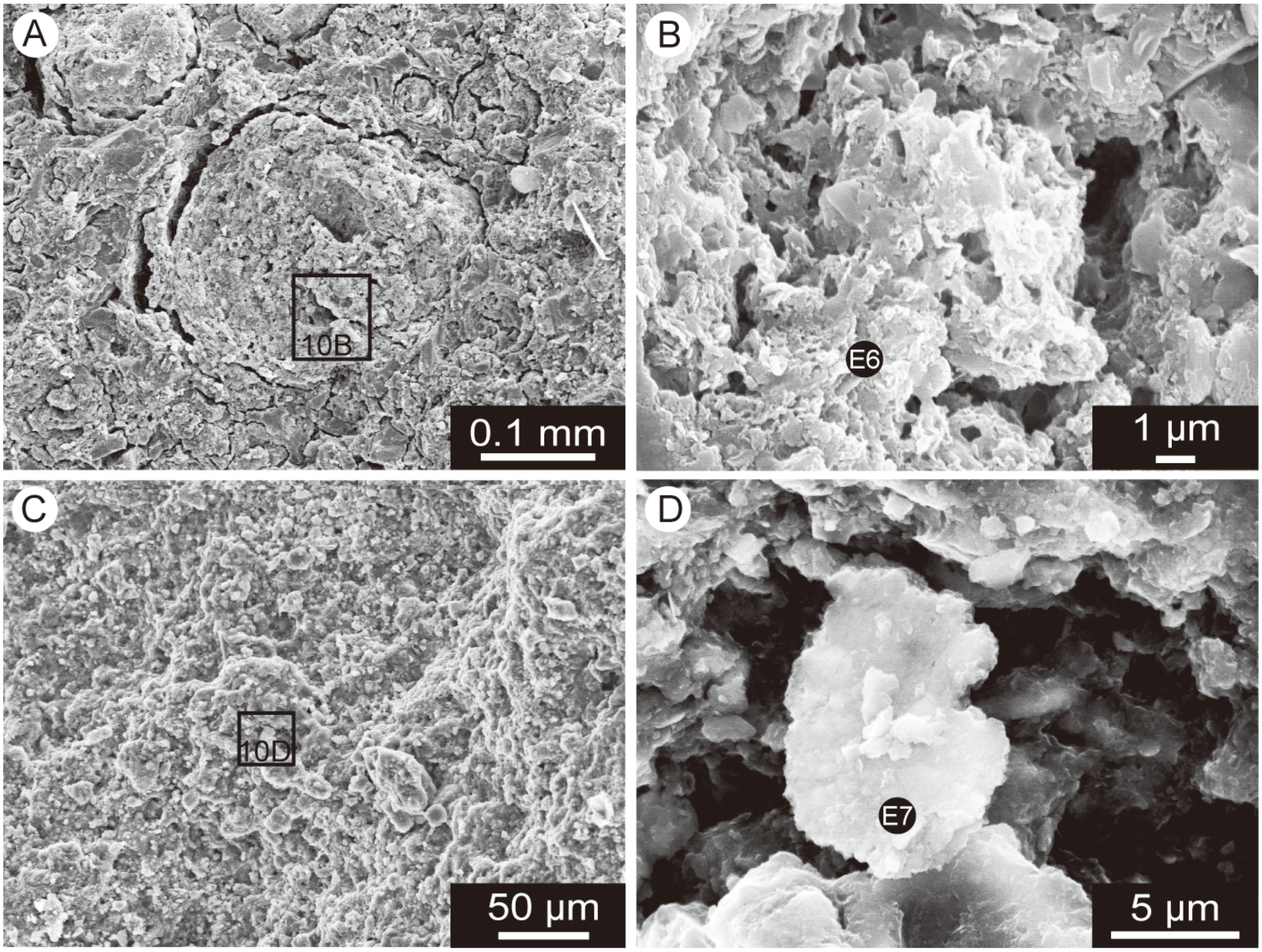
A
10B
0.1 mm
B
E6
1 μm
C
10D
50 μm
D
E7
5 μm

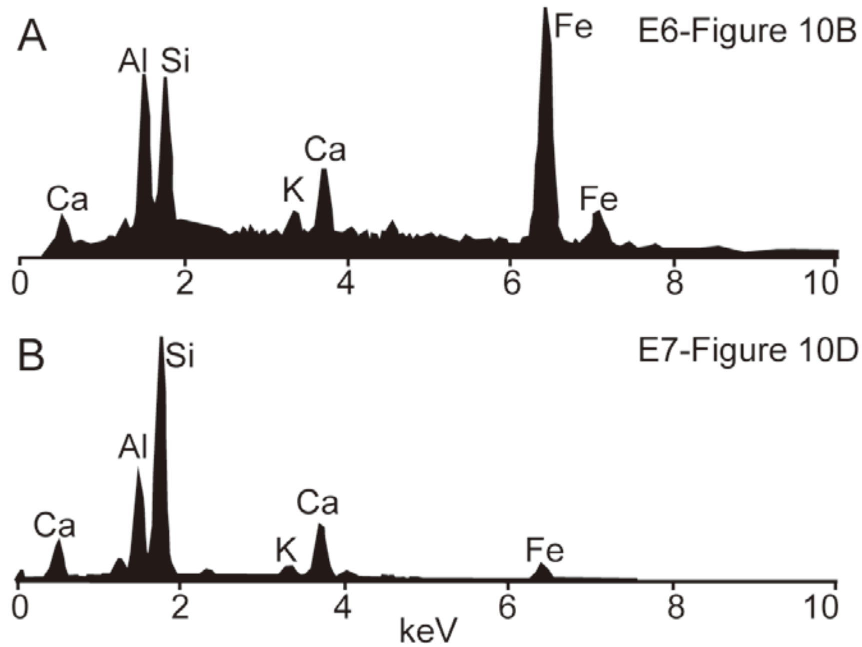
A
E6-Figure 10B
Al
Si
Fe
Ca
K
Ca
Fe
0
2
4
6
8
10
B
E7-Figure 10D
Si
Al
Ca
Ca
K
Fe
0
2
4
6
8
10
keV

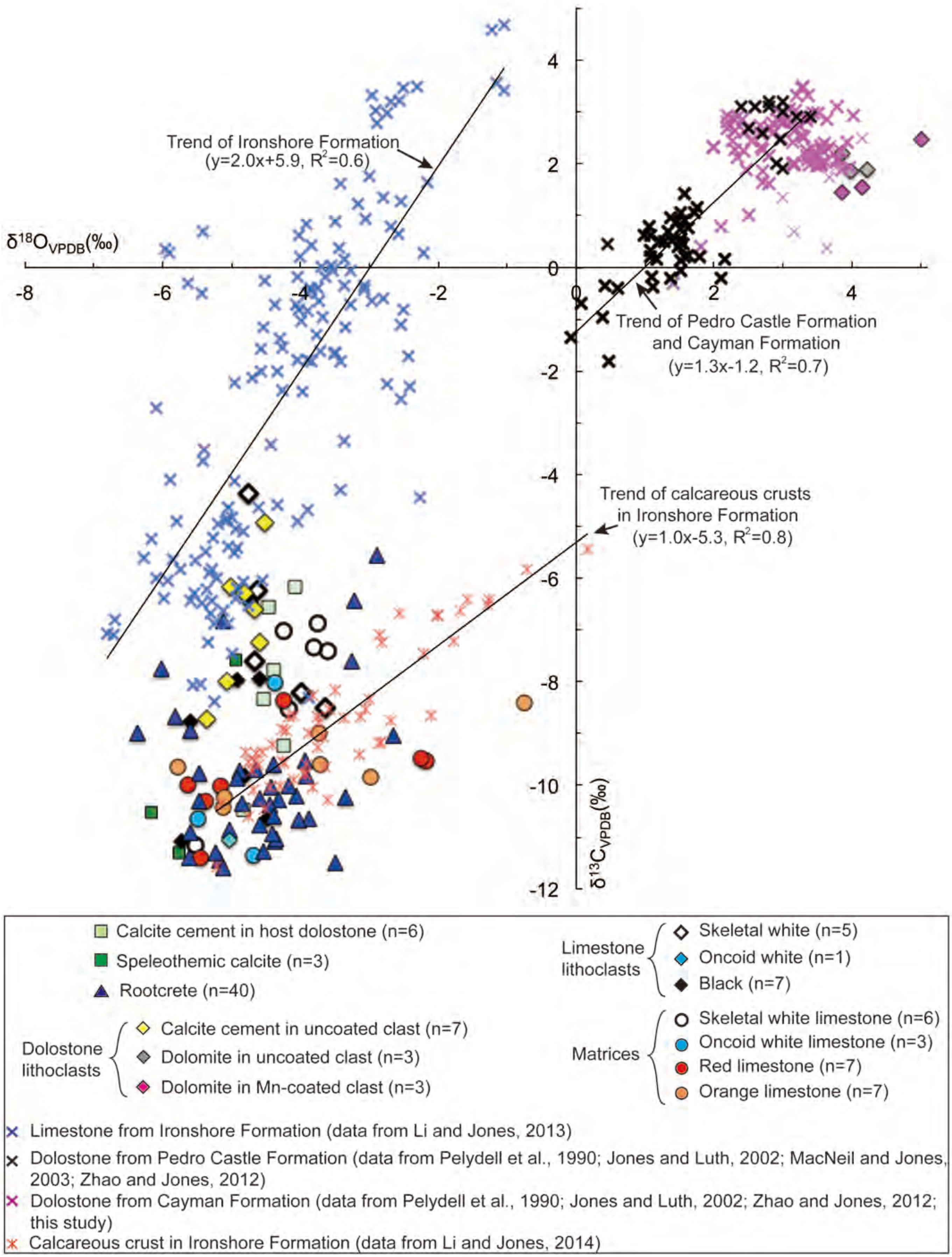

Trend of Ironshore Formation
(y=2.0x+5.9, R²=0.6)
Trend of Pedro Castle Formation
and Cayman Formation
(y=1.3x-1.2, R²=0.7)
Trend of calcareous crusts
in Ironshore Formation
(y=1.0x-5.3, R²=0.8)
δ18OVPDB(‰)
δ13CVPDB(‰)
-8
-6
-4
-2
0
2
4
-12
-10
Calcite cement in host dolostone (n=6)
Speleothemic calcite (n=3)
Rootcrete (n=40)
Dolostone lithoclasts
Calcite cement in uncoated clast (n=7)
Dolomite in uncoated clast (n=3)
Dolomite in Mn-coated clast (n=3)
Limestone lithoclasts
Skeletal white (n=5)
Oncoid white (n=1)
Black (n=7)
Matrices
Skeletal white limestone (n=6)
Oncoid white limestone (n=3)
Red limestone (n=7)
Orange limestone (n=7)
Limestone from Ironshore Formation (data from Li and Jones, 2013)
Dolostone from Pedro Castle Formation (data from Pelydell et al., 1990; Jones and Luth, 2002; MacNeil and Jones, 2003; Zhao and Jones, 2012)
Dolostone from Cayman Formation (data from Pelydell et al., 1990; Jones and Luth, 2002; Zhao and Jones, 2012; this study)
Calcareous crust in Ironshore Formation (data from Li and Jones, 2014)

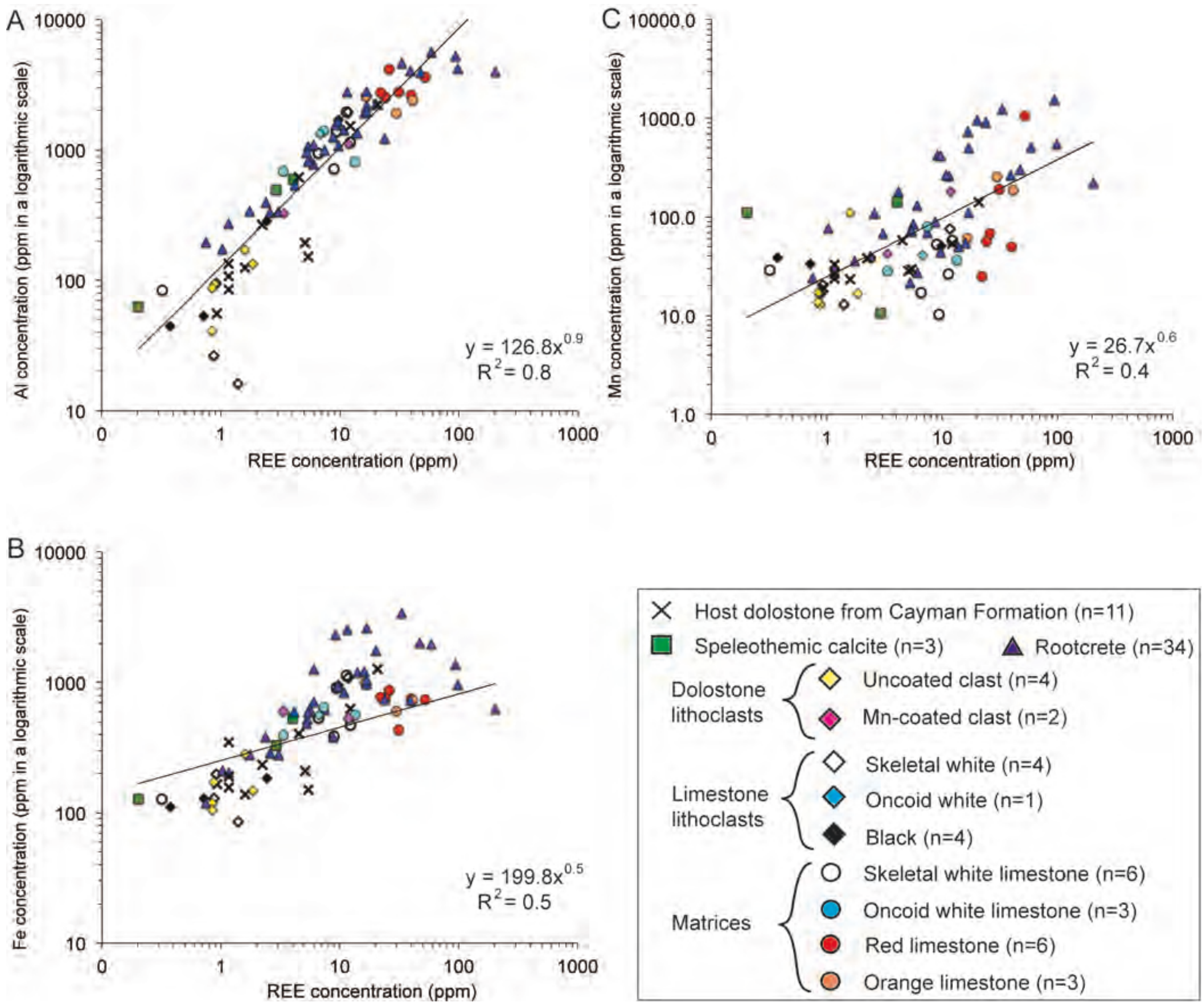
A
Al concentration (ppm in a logarithmic scale)
REE concentration (ppm)
y = 126.8x^0.9
R^2 = 0.8
B
Fe concentration (ppm in a logarithmic scale)
REE concentration (ppm)
y = 199.8x^0.5
R^2 = 0.5
C
Mn concentration (ppm in a logarithmic scale)
REE concentration (ppm)
y = 26.7x^0.6
R^2 = 0.4
Host dolostone from Cayman Formation (n=11)
Speleothemic calcite (n=3)
Rootcrete (n=34)
Dolostone lithoclasts
Uncoated clast (n=4)
Mn-coated clast (n=2)
Limestone lithoclasts
Skeletal white (n=4)
Oncoid white (n=1)
Black (n=4)
Matrices
Skeletal white limestone (n=6)
Oncoid white limestone (n=3)
Red limestone (n=6)
Orange limestone (n=3)

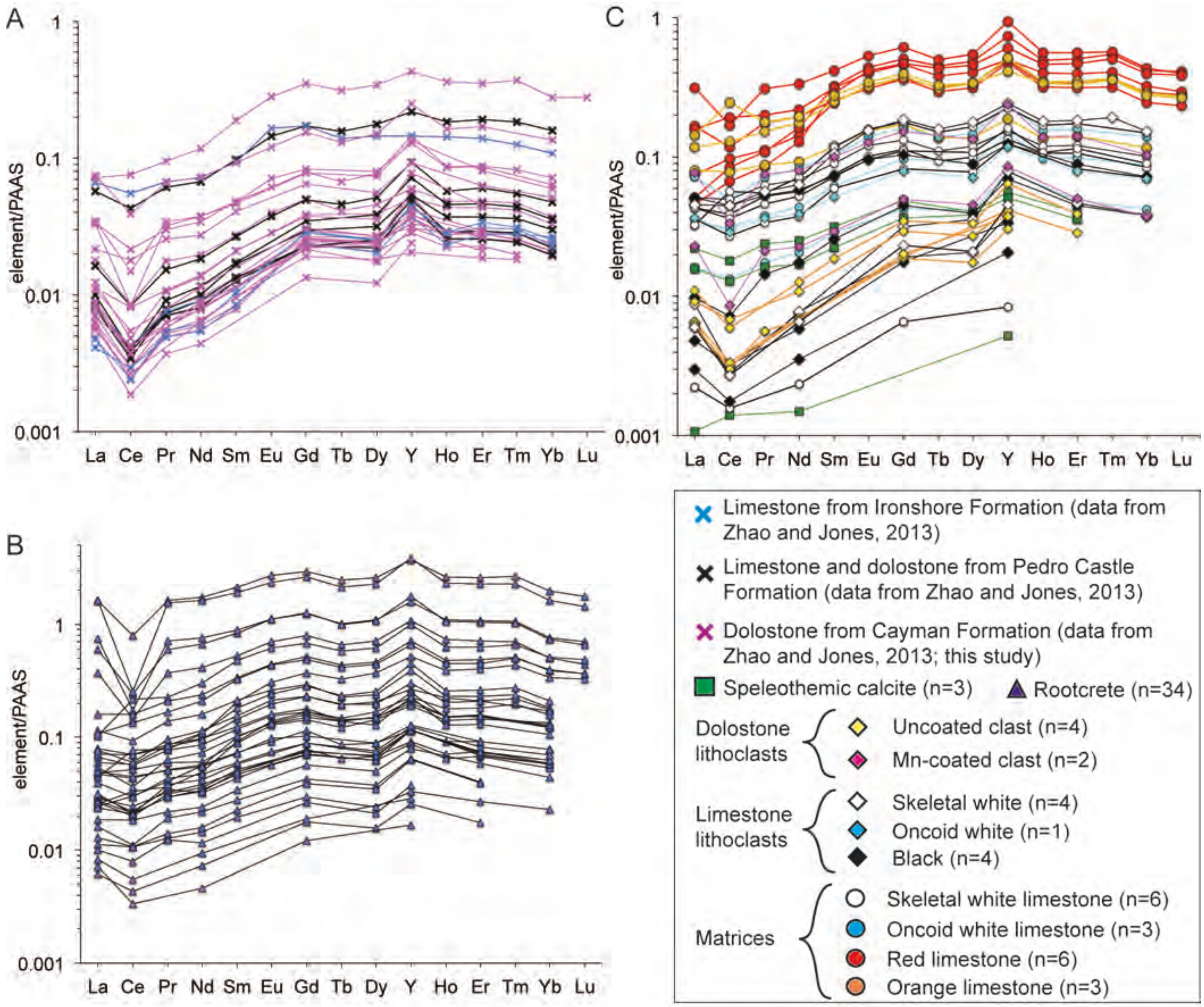

A
B
C
element/PAAS
1
0.1
0.01
0.001
La Ce Pr Nd Sm Eu Gd Tb Dy Y Ho Er Tm Yb Lu
Limestone from Ironshore Formation (data from Zhao and Jones, 2013)
Limestone and dolostone from Pedro Castle Formation (data from Zhao and Jones, 2013)
Dolostone from Cayman Formation (data from Zhao and Jones, 2013; this study)
Speleothemic calcite (n=3)
Rootcrete (n=34)
Dolostone lithoclasts
Uncoated clast (n=4)
Mn-coated clast (n=2)
Limestone lithoclasts
Skeletal white (n=4)
Oncoid white (n=1)
Black (n=4)
Matrices
Skeletal white limestone (n=6)
Oncoid white limestone (n=3)
Red limestone (n=6)
Orange limestone (n=3)

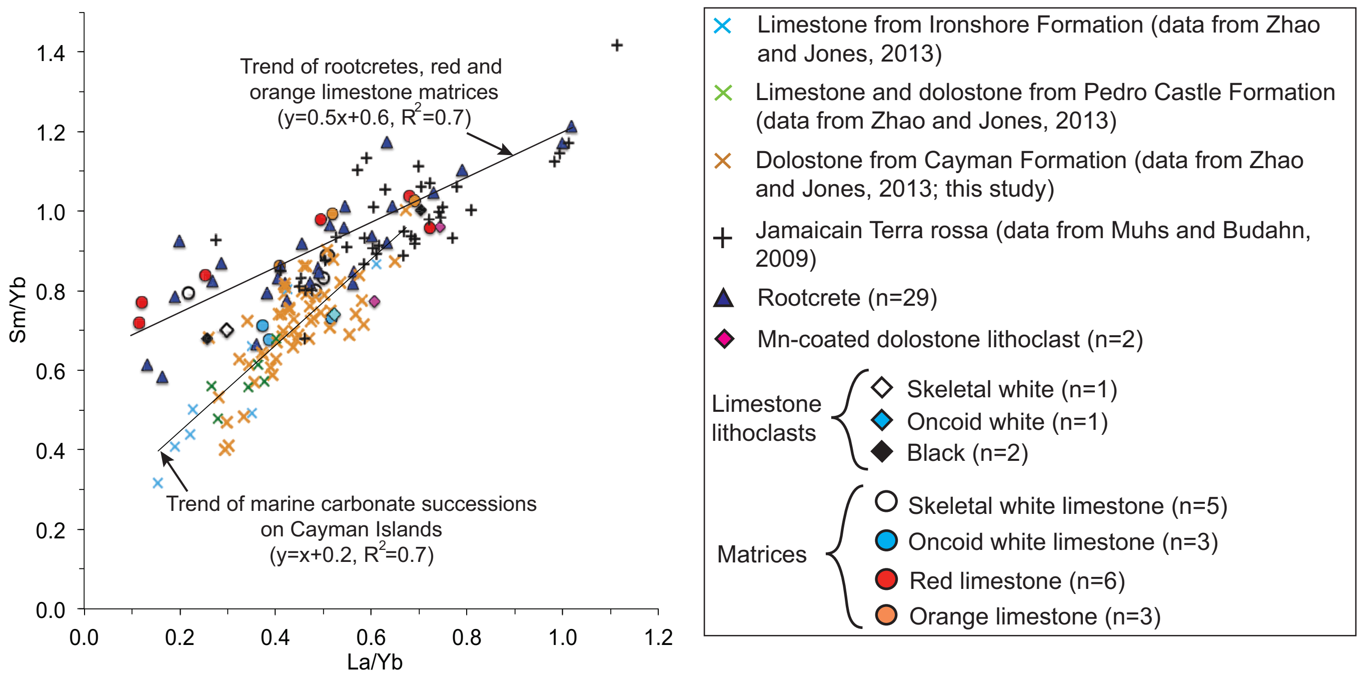

Trend of rootcretes, red and orange limestone matrices (y=0.5x+0.6, R²=0.7)
Trend of marine carbonate successions on Cayman Islands (y=x+0.2, R²=0.7)
Sm/Yb
La/Yb
0.0
0.2
0.4
0.6
0.8
1.0
1.2
1.4
Limestone from Ironshore Formation (data from Zhao and Jones, 2013)
Limestone and dolostone from Pedro Castle Formation (data from Zhao and Jones, 2013)
Dolostone from Cayman Formation (data from Zhao and Jones, 2013; this study)
Jamaicain Terra rossa (data from Muhs and Budahn, 2009)
Rootcrete (n=29)
Mn-coated dolostone lithoclast (n=2)
Limestone lithoclasts
Skeletal white (n=1)
Oncoid white (n=1)
Black (n=2)
Matrices
Skeletal white limestone (n=5)
Oncoid white limestone (n=3)
Red limestone (n=6)
Orange limestone (n=3)